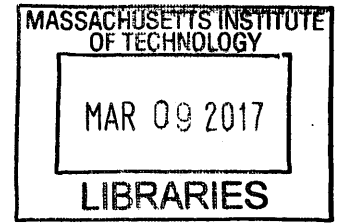


Accelerated Computational Modeling of Ballistic Helmet Test Protocols

by

Thomas Wolfgang Fronk

B.S., Massachusetts Institute of Technology (2013)



ARCHIVES

Submitted to the Department of Aeronautics and Astronautics
in partial fulfillment of the requirements for the degree of

Master's of Science in Aerospace Engineering

at the

MASSACHUSETTS INSTITUTE OF TECHNOLOGY

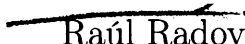
February 2017

© Massachusetts Institute of Technology 2017. All rights reserved.


Author **Signature redacted**

Department of Aeronautics and Astronautics
January 30, 2017

Certified by **Signature redacted**


Raúl Radovitzky
Professor of Aeronautics and Astronautics
Thesis Supervisor

Accepted by **Signature redacted**


Youssef M. Marzouk
Associate Professor, Aeronautics and Astronautics
Chair, Graduate Program Committee

Accelerated Computational Modeling of Ballistic Helmet Test Protocols

by

Thomas Wolfgang Fronk

Submitted to the Department of Aeronautics and Astronautics
on January 30, 2017, in partial fulfillment of the
requirements for the degree of
Master's of Science in Aerospace Engineering

Abstract

In modern combat, helmets play a vital role in protecting the head. Before being delivered to the soldier, combat helmets undergo a series of tests to determine their threat mitigation performance. During ballistic testing, current combat helmet test protocols use clay to record the helmet backface deformation signature, which is used as an important criterion to measure the helmet effectiveness at preventing head injury. However, according to a recent review of the test protocols by the National Research Council, the current test protocols establish no correlation between the backface deformation signature in the clay and head/brain injury. Modeling and simulation are valuable tools to complement experimental helmet testing and can assist in establishing this correlation. The objective of this work is to develop a comprehensive computational framework for the simulation and analysis of the helmet test protocols. In order to achieve this objective the following steps were performed. First, a suitable constitutive model for ballistic clay based on Cam-Clay theory was implemented into the computational framework SUMMIT. Next, a detailed model of the headform used in the helmet test protocols was created. The model was developed using the scanned geometry data from the experimental headform and includes the metal frame, Roma Plastilina clay and a full combat helmet with pads. Subsequently, ballistic impact simulations using the model were performed and the backface deformation signatures of the helmet are recorded in the clay. The results from these impact simulations are compared to results from impact simulations on a human head model. The intracranial pressure distribution in the human head is compared to the pressure distribution in the clay and the differences in the responses are highlighted. We conclude that the proposed computational framework is an effective tool of the analysis of helmet test protocols, which could be used to establish the correlation with injury and to guide the design of improvements to the helmet testing methodologies.

Thesis Supervisor: Raúl Radovitzky

Title: Professor of Aeronautics and Astronautics

Acknowledgments

I would like to thank my advisor, Professor Raúl Radovitzky, for giving me the opportunity to participate in this amazing research environment. I cannot express how much his guidance and support meant to me throughout my time as an undergraduate and graduate student at MIT. Working with him in his group has caused me to grow as an engineer and researcher, and I cannot emphasize enough how much I've learned.

I would also like to thank the members of the rrgroup, Dr. Khai Pham, Dr. Yang Lieu, Dr. Adrian Rosolen, Dr. Martin Hautefeuille, Dr. Aurélie Jean, Brian Fagen, Mohammad Islam and Zhiyi Wang, for their friendship and support. It was great working together and being surrounded by such great people. I'll miss our lunch breaks together!

Thank you also to our sponsors P.E.O. Soldier and to Ben for their support and guidance with the project. I enjoyed our collaboration together and am confident the project is in most capable hands.

I also would like to express my gratitude to my amazing friends at MIT, Edward Obropta, Bee Vang, Shan Shan Wang and Jackson Wirekoh. We've gone through thick and thin together and I'll miss not being around to hang out, go fishing and steal Lulu.

Also, I would like to thank MIT. My time at MIT has been truly remarkable and I'm ready to go out into the world and make a difference.

Finally, I would like to thank my parents and family for their love and support. This thesis is for you, dad!

Contents

1	Introduction	13
1.1	Background	13
1.2	Objectives and Approach	17
2	Constitutive Model of Roma Plastilina Clay	19
2.1	Model Formulation	21
2.1.1	Governing Equations	21
2.1.2	Yield criterion	25
2.1.3	Consolidation and Hardening	26
2.2	Model Implementation and Testing	26
3	Computational Framework	31
3.1	Finite Deformation Numerical Formulation	32
3.2	Solver: Newmark Scheme	33
3.3	Contact Algorithm	33
4	Model Calibration	37
4.1	Setup of the Drop Test Simulation	39
4.2	Results	42
5	Simulations of Helmet Test Protocols	49
5.1	Headform and Helmet Model Creation	51
5.2	Ballistic Impact Simulation to Record the Helmet Backface Deformation Signature in the Clay	58

5.3	Comparison between Clay Deformation/Pressure and Intracranial Pressure in the Human Head	62
6	Conclusions	69

List of Figures

1-1	ATC headform and Combat Helmet	14
2-1	Yield surface in the (p, q) -plane, preconsolidation pressure p_c and geometrical interpretation of the internal friction coefficient α	25
2-2	Hydrostatic compression test	27
2-3	Deformation of the cube subject to a triaxial compression test	29
2-4	Results of the triaxial test with different confinement pressures overlaid with the results by Ortiz/Pandolfi	30
3-1	Illustration of the penalty contact algorithm	35
3-2	Illustration of penalty algorithm	36
4-1	Comparison between the experimental drop test setup and the simulation setup	39
4-2	The clay block contains 262.000 tetrahedral elements with local refinement around the point of impact	40
4-3	Illustration of how the contact between the impacter and clay is modeled using the contact algorithm	42
4-4	Full view of drop test simulation	43
4-5	Cross section view of the drop test simulation	44
4-6	(Cross section) Final indentation depth in the clay is 25.8 mm	44
4-7	Indentation depth in the clay vs. time	45
4-8	The mesh object experiences high-localized deformation and element distortion around the impact crater	45

4-9	The high distortion of the elements reduces the quality of the elements severely	46
5-1	Current headform shape used for helmet testing	52
5-2	Unrepaired headform model	53
5-3	Repaired metal headform	54
5-4	Steps detailing the process of adding clay	55
5-5	Completed model for the headform assembling including clay and combat helmet	57
5-6	Frontal impact simulations are able to model the helmet backface deformation and record the deformation in the clay	60
5-7	Simulation results in the clay	60
5-8	The human head model captures a high amount of detail of the head and brain region	63
5-9	Ballistic impact simulation results for the clay headform and human head model	66
5-10	Pressure distributions as seen in cross-section images of the clay headform and human head model	67
5-11	The helmet backface deformation signature captured in the clay is shown along side the original undeformed clay (helmet not shown).	68

List of Tables

4.1	Optimized material parameters	42
5.1	Material parameters used for the clay in the headform assembly model	60

Chapter 1

Introduction

1.1 Background

Combat helmets play a vital role in protecting the American soldier. Helmets provide protection to the head from common threats encountered in combat zones such as fragmentation, bullets and blast. Over the past decades, helmets have undergone numerous developments and testing based on lessons learned during major conflicts.

The modern warfighter faces a variety of threats in combat zones that can lead to head injuries. In Operation Enduring Freedom in Afghanistan (OEF) and Operation Iraqi Freedom in Iraq (OIF) there were 3 major threat sources to the head: fragmentation/ballistic threats, blunt trauma and explosions. A study found that in OEF/OIF, explosions and resulting fragmentation were a major source for military wounds and dominate all other threat sources [1, 2]. A common source of such an explosion seen in those conflicts is known as an Improvised Explosive Devices (IEDs). IEDs are home made explosive devices, are cheap to make and can be packed with large amounts of shrapnel. Upon detonation this shrapnel produces a high injury threat due to fragmentation. All three types of threat sources can lead to a variety of injuries to the head region.

Injuries from ballistic and fragmentation sources include penetration trauma from a bullet or piece of shrapnel penetrating the helmet. In the case of the helmet stopping the projectile from penetrating, the resulting impact of the projectile on the helmet

can cause the helmet to deform and hit the head. This deformation is known as armor backface deformation and can result in behind armor blunt trauma. An example of behind armor blunt trauma in the civilian world is a catcher getting hit by a baseball. Although the catcher is wearing protective pads that reduce the impact of the baseball, the catcher can still suffer bruises from his pads having to absorb the kinetic energy of the baseball. In more severe cases behind armor blunt trauma on the head can cause skull fracture and trauma to the brain. Helmets and other protective headgear can reduce the injury severity to the head by absorbing some of the energy from the impact. Although the internal mechanisms causing head injury are not well understood, the helmet's ability to reduce head injury severity has led to a significant amount of research and testing to be done on helmets. The main purpose of that research and testing is to better understand and improve the effectiveness of helmets to reduce injuries to the head.



(a) ATC headform with Roma Plastilina Clay



(b) Combat Helmet

Figure 1-1: ATC headform and Combat Helmet

In order to assess this effectiveness, the helmets undergo a series of standardized ballistic and non-ballistic tests [1, 3, 4, 5, 6]. Non-ballistic tests are used to assess helmet qualities such as impact resistance, pad compression durability and compres-

sion resistance. During a ballistic test, various projectiles are fired at the helmet in order to determine the penetration resistance and the helmet's backface deformation. To set up a ballistic test, the helmet is placed on U.S. Aberdeen Test Center (ATC) headform seen in Figure 1-1a. This ATC headform is a modified version of the National Institute of Justice's headform. The ATC headform consists of a metal support frame that provides an open cavity that is filled with clay. During testing, the helmet is fastened on the headform and various projectiles are fired at the helmet and headform assembly. After impact, the clay is used as a ballistic witness material to record the test results. The highly plastic response of clay makes it suitable to record any penetration of the projectile or resulting backface deformation of the helmet after impact. The impression left in the clay due to the backface deformation signature is measured and the maximum depth is used as a criterion to evaluate the performance of the helmet.

The first published work to propose using clay, more specifically Roma Plastilina clay, as a ballistic witness material was by Prather et al. in 1977 [7, 8]. Prather et al. focused on identifying readily available means that could be used to simulate tissue response and evaluate the penetration resistance as well as the armor backface deformation of soft body armor after impact. Although not originally intended to be used for helmets, these test methodologies developed in the 70s are still largely used today for testing both body armor and helmets [9, 10]. However, according to a study conducted by the National Research Council [1], these test methodologies for combat helmets have no correlation to head and brain injury. The main concern is that the structural behavior of Roma Plastilina clay does not accurately represent the biomechanics of the human head or brain.

The structural behavior of Roma Plastilina clay can be compared to that of a granular material. A prominent characteristic of granular material is its low yield stress, particularly shear yield stress. Upon loading, this low yield stress causes Roma Plastilina clay to deform mainly plastically. As is typical with granular material, the plastic response is highly dependent on confinement pressure and loading rate. For large values of confinement pressure and high loading rates, Roma Plastilina shows a

higher resistance to compressive loading [11, 12]. The low yield stress and negligible elastic recovery upon unloading give Roma Plastilina clay the ability to record total armor deformation after testing and measure the maximum indentation depth.

However, the maximum depth in the clay caused by armor backface deformation is affected to a large degree by the state of the clay itself. Studies have shown that the maximum depth increases at elevated temperatures of the clay [12, 13]. Furthermore, the amount of deformation of the clay for a given load is also dependent on the shear history of the clay. Worked clay results in the clay being softer than non-worked clay, allowing for a higher maximum depth for a given load. Also, the clay formulation of Roma Plastilina has changed over time, which has caused variability in the loading response. In order to achieve the same rheological properties seen in the 70s, the clay now has to be heated [1]. These strong dependencies and variability in the structural response make it difficult to achieve consistent depth results in the clay after armor testing. This variability in response is detrimental to helmet testing, where the margin of error for measuring indentation depth is on the order of millimeters.

The variability in the structural response of Roma Plastilina clay has led to the implementation of conditioning and calibration procedures of the clay prior to ballistic armor testing [1]. The purpose of these procedures is to achieve consistency in the clay response across tests. After various conditioning steps that include heating the clay, the now conditioned clay is subjected to a calibration test known as the drop test. A drop test involves dropping a cylindrical impactor several times from a 2 m height onto the conditioned block of clay. The resulting maximum indentation depths in the clay are then used as a criterion to determine whether or not the clay has been appropriately conditioned. After passing the calibration test, the clay is considered ready for ballistic helmet testing.

To complement ballistic helmet testing, simulation and modeling work has been proposed. Simulation is a valuable tool to help better understand the structural responses of the helmet and clay and can offer additional insights. Simulations on the clay headform can be performed in conjunction with simulations on a human head model to better evaluate the effectiveness of helmets to prevent head injuries. Work

along these lines on human head models has been pursued in terms of blast injuries [14, 15].

In order to have a comprehensive simulation tool to model helmet test protocols there are aspects that the model needs to address. An important aspect of modeling the helmet test protocols is the correct modeling of the clay. Barring a few exceptions, the majority of current research on modeling Roma Plastilina clay involves using constitutive models that are inadequate. These are discussed in Chapter 2.

Another aspect of modeling the helmet test protocols after calibrating the clay model is developing a headform model that incorporates the clay model and uses it as a ballistic witness material. Some cases in literature have done this and have performed impact simulations on helmets and armor backed by clay [16, 17], which are described in more detail in Chapter 5.

1.2 Objectives and Approach

The objective of this work is to develop a comprehensive computational framework for the simulation and analysis of the helmet test protocols. There are several elements that make up this objective.

The first element is to make sure that a suitable constitutive model for Roma Plastilina clay is used in simulations. To this end we adopt the models presented in [18, 19, 20] based off Cam-Clay theory. Cam-Clay is suited for soil like material and captures important characteristics seen in the mechanical response of Roma Plastilina clay. The model and its implementation are presented in Chapter 2. A simulation of the drop test is used to calibrate the material parameters of the constitutive model and is presented in Chapter 4.

The second element is developing a detailed model of the headform used in the helmet test protocols. The model is developed using the scanned geometry data from the experimental headform and includes the metal frame, Roma Plastilina clay and a full combat helmet with pads. The process of developing the CAD model and mesh is described in Chapter 5.

The third element is a scalable finite element framework implementing all the necessary discretization algorithms that enable to compute the dynamics of an impact event. For this purpose we adopt the MIT/ISN SUMMIT framework that contains a large variety of capabilities that enable SUMMIT to model complex boundary value problems [21, 22, 23, 24, 25], which are described in more detail in Chapter 3. As part of simulating an impact event a contact algorithm using a penalty algorithm is implemented into SUMMIT, also presented in Chapter 3.

Combining the previously mentioned elements and tools, ballistic impact simulations using the model of the helmet test protocol are performed at two different impact locations (front and top). The impacters are modeled as small steel sphere's travelling at 200 m/s and 50 m/s. During impact, the helmet deforms and the helmet backface deformation signatures are successfully modeled in the clay part of the headform model. The resulting indentation depths in the clay are shown for both impact simulations.

A preliminary comparison between the clay response in the headform to a ballistic impact and the response of a human head is performed in an initial look at establishing a correlation between the clay response in the headform and head injuries. To achieve this, an additional ballistic impact simulation is performed on the detailed human head modeled developed by MIT and the Defense and Veterans Brain Injury Center [14]. Subsequently, the results for the intracranial pressure distribution in the human head are compared to the pressure distribution in the clay and the differences in the responses are highlighted. The ballistic impact simulations and the results are described in Chapter 5, which is followed by Conclusions and recommendations in Chapter 6.

Chapter 2

Constitutive Model of Roma

Plastilina Clay

A key ingredient in the development of a computational modeling framework for simulating the helmet test protocol is the correct description of the mechanical response of the clay. A large portion of previous research on modeling Roma Plastilina clay involves using constitutive models that are based on power law plasticity approaches [26, 27, 28, 29]. This type of models were developed and are only adequate to describe metal plasticity and do not capture important features of clay. Metals are incompressible in plasticity and have a pressure independent response, unlike soil and clay, whose structural behavior has been shown to have a high dependency on confinement pressure. A few sources in literature use constitutive models provided by commercial codes that are designed to model soil like materials [17, 16].

In this work, a constitutive model based on the Cam-Clay theory is used for modeling Roma Plastilina clay. Cam-Clay theory captures important features observed in experimental testing of Roma Plastilina clay. Features include the strong pressure dependent response, the unsymmetric response in tension vs. compression, a critical state yield behavior, as well as the ability to capture large plastic deformations.

Schofield and Wroth are the authors of the original critical state soil mechanics theory known as Cam-Clay [19]. The theory is derived from observations of soils in

laboratory tests, and it captures important structural behaviors of granular materials.

Typical soils are made out of a collection of mineral grains with pore spaces between the grains [30]. Consolidation of the soil occurs under hydrostatic compression, during which the size of the pores is irreversibly reduced, which is captured in the specific volume of the material. The amount of consolidation the soil experiences plays an important role in the subsequent structural behavior of the material. Highly preconsolidated soils have experienced a high hydrostatic loading and consequently a large reduction in pore space. These soils tend to behave more incompressible than lightly preconsolidated soils.

The preconsolidation pressure also plays a role in determining when the soil yields and controls the size of the yield surface. Larger preconsolidation pressures increase the size of the yield surface, thus increasing the elastic region of the soil. The yield surface can be characterized by three parameters: the hydrostatic pressure p , the specific volume v of the material and the deviatoric stress q . The combination of those three parameters determines if the soil has yielded. The fact that yielding is affected by the hydrostatic pressure, or confinement pressure, plays an important role in capturing the structural behavior of soil.

In practice, yield surfaces for soils are usually obtained empirically by fitting to laboratory test data. The general shape of the yield surface as defined by Schofield and Wroth is in the form of a logarithmic curve when plotted in a p, q, v space. Successive adaptations to the Cam-Clay model assume different descriptions for the general shape for the yield surface. The theory known as the Modified Cam-Clay by Roscoe and Burland describe the yield curves as continuous ellipses, allowing them to be differentiable, which is important for numerical analysis [20, 18]. The later models result in a better agreement with experiments, at the cost of complexity such as adding different finite deformation extensions and making the elastic response pressure dependent.

Upon reaching yield, the soil reaches a state known as the critical state. The critical state is characterized by the ability of the soil to sustain large plastic deformations at constant volume under constant applied shear stress. The critical state line char-

acterizes the critical state that a soil eventually reaches under sustained shearing. When plotted in a p-q space, the critical state line is a straight line passing through the origin as well as the yield surface at the location of maximum shear stress. Cam-Clay theory predicts that upon reaching the yield surface, the soil yields and follows the critical state line by either hardening or softening post yielding. Whether or not there is yield hardening or softening is determined by the amount of preconsolidation pressure and confinement pressure experienced by the soil, further emphasizing the pressure dependent response of the Cam-Clay model.

2.1 Model Formulation

As previously mentioned, different variations of the Cam-Clay theory exist in literature. The approach used in this work is the variational Cam-Clay theory of plasticity by Ortiz and Pandolfi [18]. The theory uses a general variational framework for the formulation of finite-deformation constitutive models and updates and the internal variable update is formulated as a minimization problem. The consecutive sections describe the implementation of the model and closely follow the steps presented in the paper by Ortiz and Pandolfi [18]. The steps are summarized for completeness:

2.1.1 Governing Equations

A primary assumption of the model is that the deformation gradient \mathbf{F} can be decomposed into an elastic part \mathbf{F}^e and a plastic part \mathbf{F}^p :

$$\mathbf{F} = \mathbf{F}^e \mathbf{F}^p \tag{2.1}$$

Furthermore, the flow rule is chosen to be a specific form and the yield criterion is derived, which is an approach that is suited for finite deformations. The flow rule is:

$$\dot{\mathbf{F}}^p \mathbf{F}^{p-1} = \dot{\varepsilon}^p \mathbf{M} \quad (2.2)$$

where $\dot{\varepsilon}^p$ is the effective plastic strain rate. The direction of plastic flow is defined by the tensor \mathbf{M} , which must satisfy the kinematic constraint:

$$\frac{1}{\alpha^2} (\text{tr} \mathbf{M})^2 + \frac{2}{3} \mathbf{M}^{\text{dev}} \cdot \mathbf{M}^{\text{dev}} = 1 \quad (2.3)$$

where α is an internal friction coefficient and \mathbf{M}^{dev} is the deviatoric part of \mathbf{M} . The rate sensitivity is assumed to be linear:

$$\psi^* = \frac{\eta}{2} (\dot{\varepsilon}^p)^2 \quad (2.4)$$

where η is a viscosity constant.

The elastic strain energy density W^e of the model is defined by decoupling the volumetric and the deviatoric components $W^{e,\text{vol}}$ and $W^{e,\text{dev}}$, respectively:

$$W^e(\mathbf{C}^e, T) = W^{e,\text{vol}}(J^e, T) + W^{e,\text{dev}}(\mathbf{C}^{e,\text{dev}}, T) \quad (2.5)$$

with

$$W^{e,\text{vol}}(J^e, T) = \frac{K}{2} [\theta^e - 3\alpha_T(T - T_0)]^2 + \rho_0 C_v T \left(1 - \log \frac{T}{T_0} \right) \quad (2.6)$$

and

$$W^{e,\text{dev}} = \mu |\mathbf{e}^e|^2 \quad (2.7)$$

where \mathbf{C}^e is the elastic right-Cauchy Green deformation tensor, T is temperature, T_0 is a reference absolute temperature, J^e is the Jacobian of the elastic deformation, θ^e is the elastic volumetric strain, K is the isothermal bulk modulus, α_T is the thermal expansion coefficient, ρ_0 is the mass density per unit undeformed volume, C_v is the specific heat per unit mass, μ is the shear modulus and \mathbf{e}^e the deviatoric logarithmic elastic strain.

The free energy of the system has the form [31]:

$$A(\mathbf{F}, \mathbf{F}^p, T, \varepsilon^p) = W^e(\mathbf{C}^e, T) + W^p(T, \varepsilon^p, \theta^p) \quad (2.8)$$

where W^p is the stored energy and θ^p is the volumetric plastic strain.

Discretization of the system allows for solving for incremental deformations in Δt time steps. This is achieved by defining an incremental energy function using logarithmic elastic strains [31, 32]:

$$\begin{aligned} f_n(\mathbf{F}_{n+1}, T_{n+1}; \Delta \boldsymbol{\varepsilon}^p) = \\ W^e(\boldsymbol{\varepsilon}_{n+1}^{e, \text{pre}} - \Delta \boldsymbol{\varepsilon}^p, T_{n+1}) + W^p(T_{n+1}, \varepsilon_{n+1}^p, \theta_{n+1}^p) + \Delta t \psi^*(\Delta \varepsilon^p / \Delta t) \end{aligned} \quad (2.9)$$

where $\boldsymbol{\varepsilon}_{n+1}^{e, \text{pre}}$ is the predictor of the elastic strain. and the incremental plastic strain:

$$\Delta \boldsymbol{\varepsilon}^p = \Delta \varepsilon^p \mathbf{M} \quad (2.10)$$

By minimizing f_n with respect to the effective plastic strain ε_{n+1}^p and the direction of plastic flow \mathbf{M} , an effective work-of-deformation density is defined:

$$W_n(\mathbf{F}_{n+1}, T_{n+1}) = \min_{\varepsilon_{n+1}^p, \mathbf{M}} f_n(\mathbf{F}_{n+1}, T_{n+1}; \varepsilon_{n+1}^p, \mathbf{M}) \quad (2.11)$$

Using this formulation, the First Piola-Kirchoff stress tensor can be obtained according to [31, 32]:

$$\mathbf{P}_{n+1} = \frac{\partial W_n}{\partial \mathbf{F}_{n+1}}(\mathbf{F}_{n+1}, T_{n+1}) \quad (2.12)$$

After various derivation steps [18] and decomposing the stress into the volumetric stress component p_{n+1}^{pre} and the deviatoric stress component q_{n+1}^{pre} , a system of equations can be defined:

$$q_{n+1}^{\text{pre}} = (3\mu \Delta \varepsilon^p + \sigma_{0, n+1} + \psi^{*'}) \cos \phi \quad (2.13)$$

$$p_{n+1}^{\text{pre}} = p_{0, n+1} + [\alpha K \Delta \varepsilon^p + (\sigma_{0, n+1} + \psi^{*'}) / \alpha] \sin \phi \quad (2.14)$$

where $\sigma_{0,n+1}$ is the critical uniaxial stress and $p_{0,n+1}$ is the critical pressure.

After linearizing this system of equations, a Newton-Raphson iteration is used to solve for the incremental plastic strain $\Delta\varepsilon^p$ and phase angle ϕ . The linearized system of equations is:

$$dq_{n+1}^{\text{pre}} = C_{11}d\varepsilon_{n+1}^p + C_{12}d\phi \quad (2.15)$$

$$dp_{n+1}^{\text{pre}} = C_{21}d\varepsilon_{n+1}^p + C_{22}d\phi \quad (2.16)$$

where

$$C_{11} = \left(3\mu + \frac{\psi^{*''}}{\Delta t} + H_{\varepsilon\varepsilon,n+1} + \alpha H_{\varepsilon\theta,n+1} \sin \phi \right) \cos \phi \quad (2.17)$$

$$C_{12} = \alpha H_{\varepsilon\theta,n+1} \Delta\varepsilon^p \cos^2 \phi - (3\mu \Delta\varepsilon^p + \sigma_{0,n+1} + \psi^{*'}) \sin \phi \quad (2.18)$$

$$C_{21} = H_{\theta\varepsilon,n+1} + \left(\alpha K + \frac{\psi^{*''}}{\alpha \Delta t} + \alpha H_{\theta\theta,n+1} + \frac{1}{\alpha} H_{\varepsilon\varepsilon,n+1} + H_{\varepsilon\theta,n+1} \sin \phi \right) \sin \phi \quad (2.19)$$

$$C_{22} = \left(\alpha H_{\theta\theta,n+1} \Delta\varepsilon^p + H_{\varepsilon\theta,n+1} \Delta\varepsilon^p \sin \phi + \left[\alpha K \Delta\varepsilon^p + \frac{1}{\alpha} (\sigma_{0,n+1} + \psi^{*'}) \right] \right) \cos \phi \quad (2.20)$$

and

$$H_{\theta\theta} = \frac{\partial p_0}{\partial \theta^p} = \frac{\partial^2 W^p}{\partial \theta^p \partial \theta^p}(\theta^p, \varepsilon^p) \quad (2.21)$$

$$H_{\theta\varepsilon} = \frac{\partial p_0}{\partial \varepsilon^p} = \frac{\partial^2 W^p}{\partial \theta^p \partial \varepsilon^p}(\theta^p, \varepsilon^p) \quad (2.22)$$

$$H_{\varepsilon\theta} = \frac{\partial \sigma_0}{\partial \theta^p} = \frac{\partial^2 W^p}{\partial \varepsilon^p \partial \theta^p}(\theta^p, \varepsilon^p) \quad (2.23)$$

$$H_{\varepsilon\varepsilon} = \frac{\partial\sigma_0}{\partial\varepsilon^p} = \frac{\partial^2 W^p}{\partial\varepsilon^p \partial\varepsilon^p}(\theta^p, \varepsilon^p) \quad (2.24)$$

2.1.2 Yield criterion

The yield criterion is:

$$q^2 + \alpha^2(p - p_0)^2 = \sigma_0^2 \quad (2.25)$$

As seen in Figure 2-1 taken from [18], the resulting yield surface forms an ellipse centered around p_0 . The point of maximum pressure on the yield surface is defined as the preconsolidation pressure p_c .

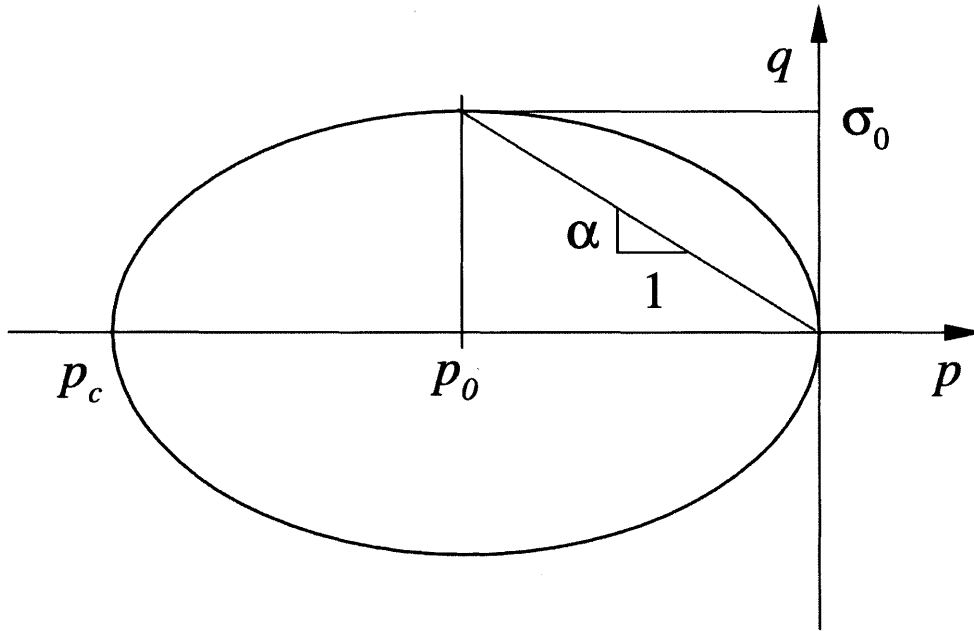


Figure 2-1: Yield surface in the (p, q) -plane, preconsolidation pressure p_c and geometrical interpretation of the internal friction coefficient α

2.1.3 Consolidation and Hardening

The harding characteristics of the model are determined by the consolidation curve, which is assumed to be of the form [18, 30]:

$$p_c = p_{\text{ref}} \sinh \frac{\theta^p}{\theta_{\text{ref}}^p} \quad (2.26)$$

Where p_{ref} and θ_{ref}^p are material constants. Using 2.26 the stored energy function is:

$$W_c^p(\theta^p) = \int_0^{\theta^p} p_c d\theta^p = p_{\text{ref}} \theta_{\text{ref}}^p \left(\cosh \frac{\theta^p}{\theta_{\text{ref}}^p} - 1 \right) \quad (2.27)$$

2.2 Model Implementation and Testing

The Cam-Clay material model described in Ortiz and Pandolfi's paper [18] was implemented into SUMMIT, which is described in more detail in Chapter 3. A series of simple tests at a constitutive/low level are performed. The purpose of these tests is to verify that the Cam-Clay material model is successfully implemented into SUMMIT and the results from these verification tests are compared to results and observations given by the original authors of this Cam-Clay formulation [18].

The first verification test is a hydrostatic compression test. During a hydrostatic compression test, the material is compressed in the three principal stress directions. This test is performed at a constitutive level using one quadrature point. For a test at a constitutive level, the user provides the deformation gradient and receives the stress tensor resulting from that deformation tensor. In the case of a hydrostatic compression test, the deformation gradient is known (Equation 2.28):

$$\mathbf{F} = \begin{pmatrix} \lambda & 0 & 0 \\ 0 & \lambda & 0 \\ 0 & 0 & \lambda \end{pmatrix} \quad (2.28)$$

where

$$\lambda = 1 - 10dt \quad (2.29)$$

where dt is one time step specified in the test setup

As seen in Figure 2-2, during hydrostatic compression, the material behaves first elastically at small volumetric strains. After reaching the yield point, the pressure grows in a nonlinear fashion with increasing volumetric strains. This behavior is consistent with the findings provided by the original authors of the model [18].

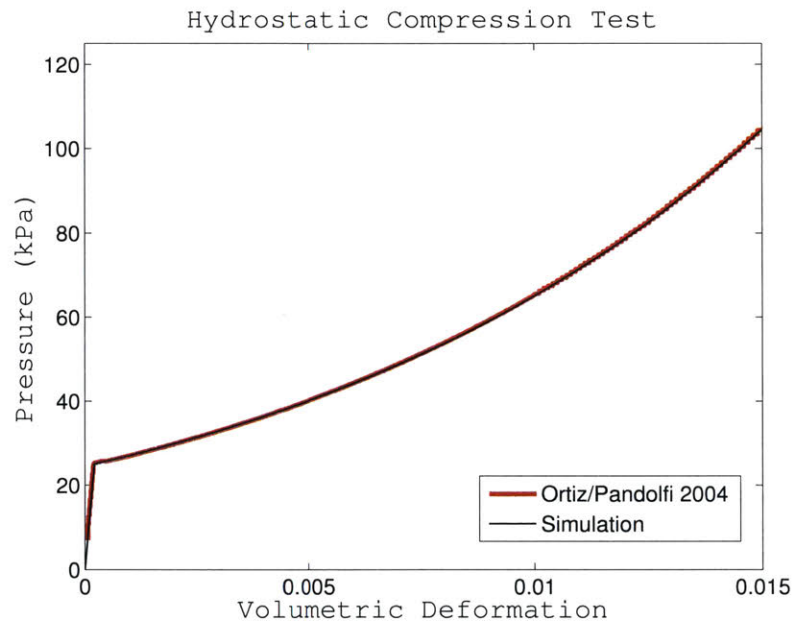


Figure 2-2: Hydrostatic compression test

The second verification test is a triaxial compression test. A triaxial compression test is commonly performed on soil like materials, such as rock and clay, and is used as a method to determine the mechanical properties of soils. During a triaxial test the material is subjected to a hydrostatic confinement pressure, which is followed by uniaxial compression in one direction. The additional uniaxial compression causes the stress in that direction to be greater than the stress along the other two axes, which results in a shear stress in the material. Contrary to the hydrostatic compression test, the triaxial test could not be performed at a constitutive level using only one

quadrature point. The reason is that for a test using a single quadrature point, the user must provide a known deformation gradient in order to receive the resulting stress tensor. The deformation gradient corresponding to a triaxial compression test using Cam-Clay is not known. Thus the triaxial test is performed as a three-dimensional boundary value problem using a simple cube mesh object.

The cube contains 8 symmetric tetrahedral elements. In order to simulate a triaxial test, the boundary conditions on the 6 faces of the cube are defined accordingly. A Neumann pressure boundary condition is set for 2 neighboring faces, while a Dirichlet roller boundary condition is set for the opposing faces. The boundary conditions on these 4 faces (i.e. “side” faces) are used to describe the confinement pressure of a triaxial test. The remaining 2 faces, which are opposite of one another (i.e. “top” and “bottom” faces), have Dirichlet boundary conditions that serve to describe the uniaxial compression during a triaxial test.

There are two reasons why this setup is not ideal. The first reason is that the confinement pressure is not applied to the top and bottom faces. The user cannot specify both a Dirichlet and Neumann boundary condition at the same time pointing in the same direction on the same face. However, during uniaxial compression of the cube, which occurs by applying the Dirichlet boundary conditions on the top and bottom surface, the cube eventually reaches a state where the displacement set by Dirichlet boundary conditions corresponds to the displacement the cube would have seen due to the confinement pressure being applied on those surfaces.

The second reason this setup is not ideal is that a cube instead of a cylindrical shaped object is used for the triaxial test simulation. A cylinder is the shape usually chosen for an experimental triaxial test specimen, as the sharp corners of a cube pose challenges in applying the correct confinement pressure. The reason a cube is chosen in this work is its simplicity and ability to still capture the important features of the structural behavior of the Cam-Clay model subjected to a triaxial test.

For a triaxial test, the Cam-Clay theory predicts the following structural behavior. Upon reaching yield, the material softens for low values of confinement pressure and hardens for high values of confinement pressure. The hardening or softening occurs

until the material reaches the critical state after which it behaves nearly perfectly plastic. Figure 2-3 shows the deformation of the cube subject to a triaxial compression test. The cube is compressed on the top and bottom surfaces resulting in a reduction of height and increase in width.

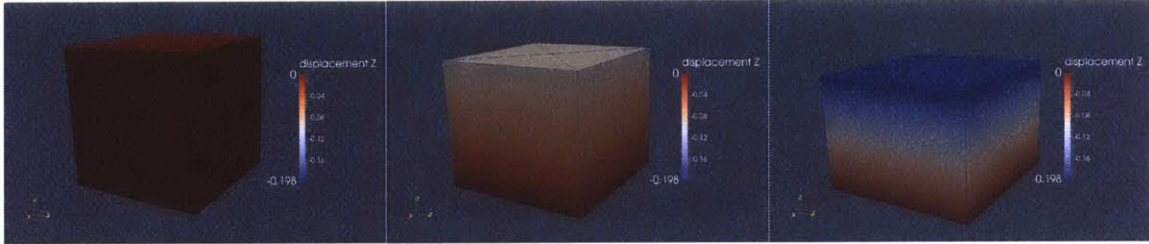


Figure 2-3: Deformation of the cube subject to a triaxial compression test

In Figure 2-4 the true axial stress and true axial strain results are plotted. The original results from Ortiz and Pandolfi's paper are overlaid in the graph [18]. As shown, the results show a good correlation with each other. The difference in final slope is most likely due to the fact that the triaxial test in this work is performed on a three dimensional boundary value problem level using a cube instead of on a constitutive level.

Other tests including a shear test were conducted to further verify the correct implementation of the model. These tests are not described in this work since although they support the conclusion that the model has been successfully implemented into SUMMIT, they do not add any additional insights to the verification process.

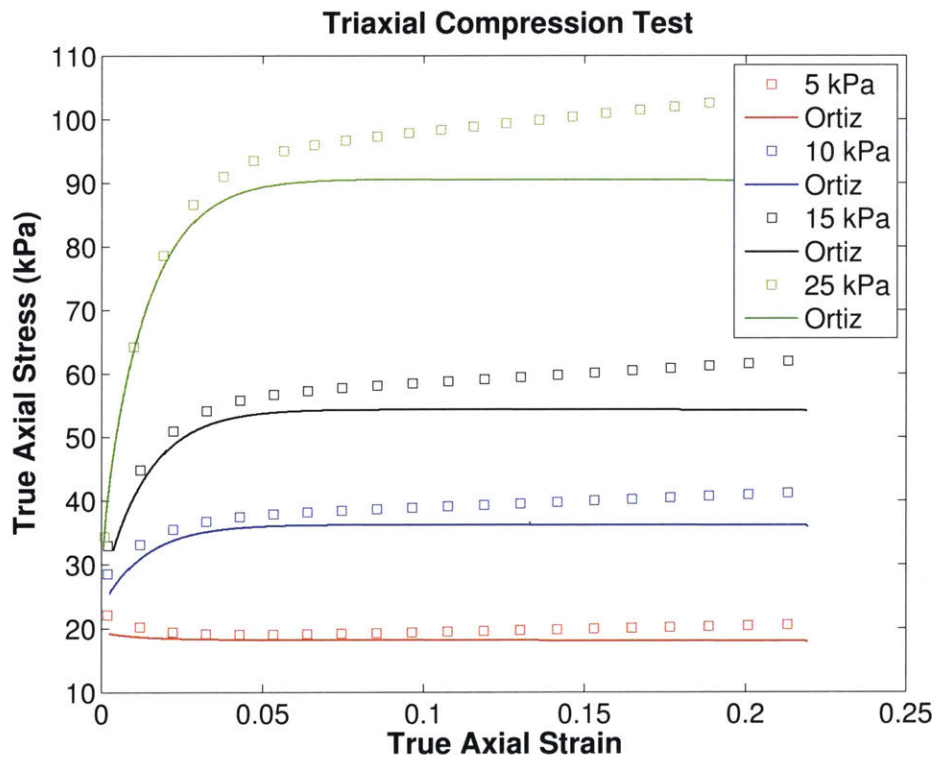


Figure 2-4: Results of the triaxial test with different confinement pressures overlaid with the results by Ortiz/Pandolfi

Chapter 3

Computational Framework

In this work SUMMIT is used to perform the ballistic impact simulations on the model of the helmet test protocols. SUMMIT is a computational framework for solid mechanics and was developed by the research group headed by Professor Raul Radovitzky. SUMMIT is dedicated to large-scale simulations for materials and structures. Its capabilities include continuous and discontinuous Galerkin methods, multi-scale simulations, explicit dynamics and higher order methods [24, 25]. These capabilities enable SUMMIT to model complex boundary value problems involving fracture using discontinuous Galerkin methods [21, 22, 23, 24, 25]. SUMMIT is also able to run large scale simulations in parallel. The ability to use parallel computation is very valuable in performing the simulations described in this work and significantly reduces the amount of time required to run the simulations.

SUMMIT has an extensive material library that contains a large variety of validated constitutive models. SUMMIT also provides the capability to incorporate and implement new material models into its material library. This capability enabled the constitutive model for Cam-Clay described in Ortiz and Pandolfi's paper [18] to be implemented into SUMMIT and subsequently used for this work to model Roma Plastilina clay.

3.1 Finite Deformation Numerical Formulation

In this section, the underlying mathematical formulations are described, in particular regarding modeling finite deformations.

The deformation gradient tensor \mathbf{F} of a body relates the deformation in the current configuration to the reference configuration,

$$F_{ij} = \frac{d\mathbf{x}_i}{d\mathbf{X}_j} = \frac{\partial\varphi_i}{\partial\mathbf{X}_j} \quad (3.1)$$

where \mathbf{X}_j is the material point in the reference geometry, \mathbf{x}_i is the material point in the current displacement geometry, and $\varphi(\mathbf{X}, t)$ the Lagrangian description of the displacement vector using material coordinates.

The Jacobian of the deformation gradient tensor relates the change in volume in the current configuration to the volume in the reference configuration and is defined as the determinant of \mathbf{F} ,

$$J = \det\mathbf{F} \quad (3.2)$$

The First Piola-Kirchhoff stress tensor expresses stress relative to the reference configuration and relates forces in the current configuration with areas in the reference configuration. The relationship between the First Piola-Kirchhoff stress tensor and the Cauchy stress tensor is the following,

$$P_{ij} = J\sigma_{ik}F_{kj}^{-T} \quad (3.3)$$

Where P is the First Piola-Kirchhoff stress tensor, σ is the Cauchy stress tensor.

For a body B_0 subjected to a force per unit mass \mathbf{B} , with a Dirichlet boundary surface portion $\partial_D B_0$ and a Neumann part $\partial_N B_0$, the problem is governed by the linear momentum balance equation,

$$\rho_0\ddot{\varphi} = \nabla_0 \cdot \mathbf{P}^T + \rho_0\mathbf{B} \text{ in } B_0 \quad (3.4)$$

Where ρ_0 is the initial density and $\ddot{\varphi}$ is the acceleration. Equation 3.4 is expressed

in the strong form [23]. The weak form can be obtained by multiplying by a test function φ_h and integrating over the domain:

$$\sum_e \int_B (\rho_0 \ddot{\varphi}_h \cdot \delta \varphi_h + \mathbf{P}_h : \nabla_0 \delta \varphi_h) dV = \sum_e \int_B \rho_0 \mathbf{B} \cdot \delta \varphi_h dV + \sum_e \int_{\delta_{NB}} \delta \varphi_h \cdot \bar{\mathbf{T}} dS \quad (3.5)$$

where \mathbf{P}_h is the discretized stress tensor and $\bar{\mathbf{T}}$ is the surface traction.

3.2 Solver: Newmark Scheme

The numerical solver used in this work to evaluate the dynamic response of solids is the lumped mass matrix Newmark method expressed in equations 3.6, 3.7 and 3.8, with the Newmark parameters β and γ set to 0 and 0.5, respectively.

$$\mathbf{x}_a^{n+1} = \mathbf{x}_a^n + \Delta t \dot{\mathbf{x}}_a^n + \Delta t^2 \left[\left(\frac{1}{2} - \beta \right) \ddot{\mathbf{x}}_a^n + \beta \ddot{\mathbf{x}}_a^{n+1} \right] \quad (3.6)$$

$$\dot{\mathbf{x}}_a^{n+1} = \dot{\mathbf{x}}_a^n + \Delta t [(1 - \gamma) \ddot{\mathbf{x}}_a^n + \gamma \ddot{\mathbf{x}}_a^{n+1}] \quad (3.7)$$

$$\ddot{\mathbf{x}}_a^{n+1} = \mathbf{M}_{ab}^{-1} [\mathbf{f}^e - \mathbf{f}^i]_b^{n+1} \quad (3.8)$$

where \mathbf{x} is, Δt is the time step, \mathbf{M} is the lumped mass matrix, \mathbf{f}^e is the external force, and \mathbf{f}^i is the internal force.

3.3 Contact Algorithm

A contact algorithm is used in the ballistic simulations described in Chapter 4 and 5. The contact algorithm described in this section is a key feature that is required to prevent interpenetration of bodies that come into contact and is used to determine the contact forces.

A variety of algorithms in literature exist to solve contact problems using finite

element simulations [33]. The two most common algorithms are the Lagrange multiplier method and the penalty method. While the Lagrange method can lead to better results for contact problems in certain situations, the penalty method is often the more popular choice. This is due to the simple and robust nature of penalty algorithms. An important consideration when using a penalty algorithm is the correct choice for the penalty parameter. The penalty parameter determines the amount of contact force that is generated during contact and is set by the user. A bad value for the penalty parameter can lead to an ill-conditioned system and inaccurate simulation results. A too low value for the penalty parameter can lead to the contacting bodies interpenetrating, while a too high value can lead to instability in the simulation.

In this work we adopt a contact algorithm based on penalty methods. For a given simulation, the contact algorithm is setup to include an impacter and a mesh object. The impacter is modeled as a rigid sphere that cannot deform on contact with the mesh object. The radius and mass of the sphere are set by the user and remain constant throughout the simulation. The user also provides the initial position of the center of the sphere relative to the mesh object as well as the initial velocity of the sphere.

At every time step in the simulation, the contact algorithm loops over all the quadrature points located on the surface of the mesh object and determines their position relative to the position of the center of the rigid sphere. If the distance, \mathbf{d} , between the positions of each quadrature point and the position of the center of the sphere is more than the radius of the sphere, then there is no contact and the contact algorithm does nothing. If, however the distance between one or several quadrature points is less than the radius of the sphere, the impacter and the mesh object are in contact and the contact algorithm determines the resulting contact force.

An illustration of this process is as follows. The amount of contact, or interpenetration **delta** (δ), that a quadrature point has with the sphere is calculated by subtracting the distance \mathbf{d} , which is the distance between that quadrature point and the center of the sphere, with the radius of the sphere \mathbf{r} (Figure 3-1).

The amount of interpenetration δ is multiplied by the given penalty parameter

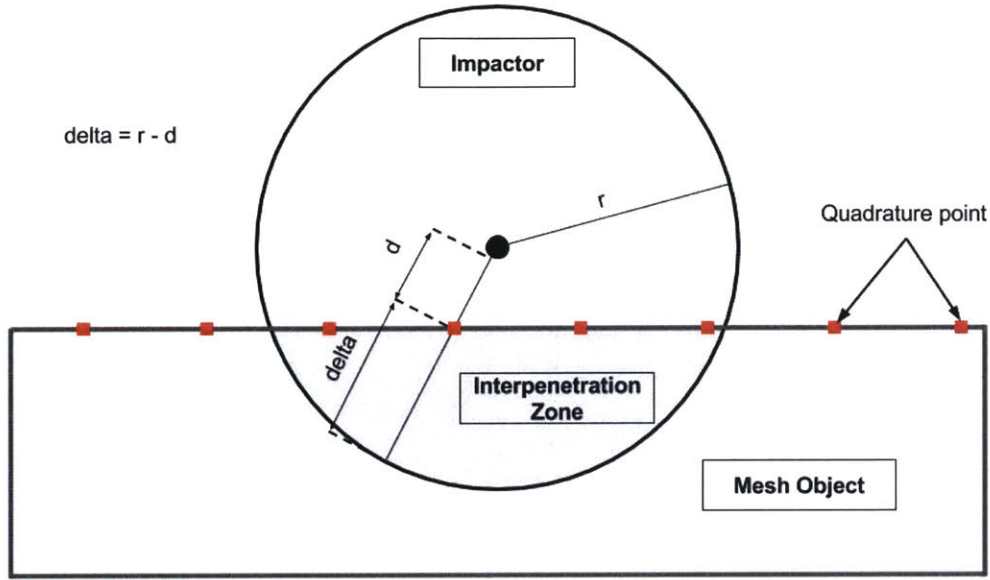


Figure 3-1: Illustration of the penalty contact algorithm

p to determine the resulting initial magnitude of the contact force $F_{penalty}$ that is assigned to that quadrature point (see Figure 3-2 Equation 3.9).

$$F_{penalty} = \delta * p \quad (3.9)$$

This process is repeated for each quadrature point that is in contact with the sphere (Figure 3-2). Before applying the individual contact forces to the quadrature points, the initial contact forces are weighed and their magnitudes are adjusted according to the sizes of the elements the quadrature points belong to. After this weighing process the forces are applied to each quadrature point as Neumann boundary conditions. The resulting directions of the force vectors applied to each quadrature point are pointing away from the center of the sphere, causing the mesh object to deform away from the sphere.

The reaction force acting on the the sphere is equal and opposite to the assembled forces seen by the mesh object and the reaction force is used to compute the dynamics of the sphere according to Newton Laws (Figure 3-2).

In the next time step, the new position of the impactor and the deformation state

of the mesh object are known, and the time integration continues until the final simulation time is reached.

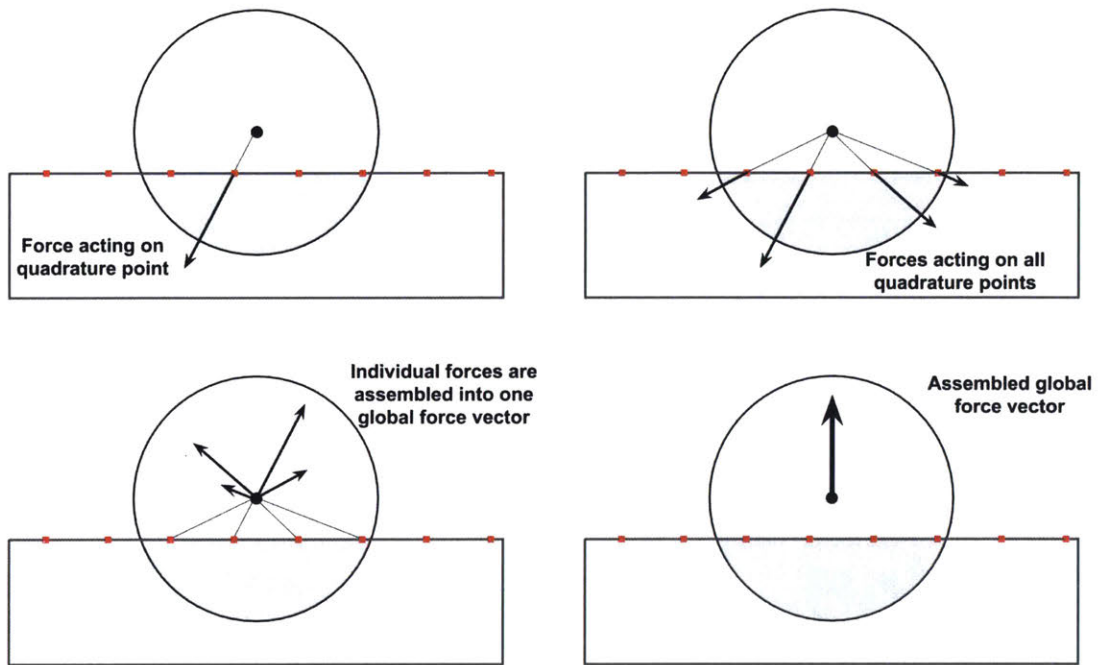


Figure 3-2: Illustration of penalty algorithm

Chapter 4

Model Calibration

In the process of implementing a constitutive model it is critical to calibrate the material parameters.

The constitutive model for Roma Plastilina clay described in Chapter 2 has 11 material parameters, some of which have physical meaning and some don't. The material parameters which have a physical meaning are the density ρ , Young's Modulus E , Poisson's ratio ν , preconsolidation pressure P_c , rate sensitivity parameter η , friction angle, reference temperature, thermal expansion coefficient and specific heat/unit mass. The last three (reference temperature, thermal expansion coefficient and specific heat/unit mass) model the thermal dependencies and effects of the material. For this work, it is assumed that the Roma Plastilina clay has been heated to and remains at the temperature at which it is used for experimental helmet testing. Thus thermal effects are not considered in the analysis and the thermal parameters of the material model do not need to be calibrated. Of the remaining 8 material parameters, the preconsolidation pressure and friction angle are parameters inherent to Cam-Clay theory and model pressure dependency and friction. The reference volumetric strain V_{ref} and the reference pressure P_{ref} are the two material parameters that do not have a direct physical meaning and are used in conjunction with the preconsolidation pressure to set the pressure dependency of the model.

To calibrate a constitutive model, ideally simple tests such as a uniaxial compression test are used to obtain constitutive data. The resulting stress-strain curves can

be used to isolate and calibrate the individual material parameters one at a time. After an extensive literature review, it is found that such constitutive level tests have almost exclusively been performed on non-Roma Plastilina clay or on non-conditioned clay in order to calibrate J2 plasticity models [26, 28, 29]. This was inadequate for this work.

An alternative method to calibrate a model when constitutive data is not available is to use more complex tests that result in compound material responses. From a mathematical perspective these tests are boundary value problems in which the material has a multitude of states. Rather than using the stress-strain response at any point in the material to calibrate individual material parameters a metric observed in the global response is chosen and the material parameters are configured in order to achieve the experimental results of that metric. However, the resulting set of parameters that would fit that metric are most likely not unique.

Although the approach using simple tests is more desirable, due to lack of adequate experimental results for Roma Plastilina clay, a complex test known as the drop test is used to calibrate the Cam-Clay model in this work. In the following paragraphs the details of the drop test and the metric used to calibrate the clay are described.

Prior to experimental ballistic helmet testing, the drop test is used to verify that the clay has been appropriately conditioned (see Chapter 1). To set up a drop test specified by the helmet test protocols the conditioned clay is filled into a 0.305 m wide by 0.305 m long by 0.1 m high aluminum/wooden box. A 1 kg cylindrical steel mass with a hemispherical end is dropped from a 2 m height onto the clay. After impact, the steel mass is removed and the final indentation depth in the clay is measured and used as a calibration metric. This process is repeated two additional times for a total of 3 drops on one block of clay. In order for the clay to pass the drop test calibration test, all three final indentation depths in the clay have to be 25.4 ± 2.5 mm respectively.

In literature, simulations of a variety of drop tests are performed and the final indentation depth in the clay is used as a metric to calibrate their respective constitutive models [17, 16, 26, 27]. In some cases, the drop test setup is varied to include dif-

ferent impacter weights and drop heights [26, 27]. Using a range of impacter weights and drop heights allows the calibration of the constitutive model to take into account the loading rate dependency characteristic of Roma Plastilina clay. Buchely et al. perform several drop tests with different setups and analyze the indentation depth of the impacter vs. time [26]. The experimental indentation depth results vs. time show a gradual decrease of the rate of indentation depth with no indication of an elastic recovery of the clay.

The drop test simulation used in this work to calibrate the constitutive model is setup according to the experimental setup specified by the helmet test protocols described above. In addition to using the final indentation depth in the clay as a calibration metric, the indentation depth vs. time and the shape of the clay are used. The subsequent section describes the simulation setup.

4.1 Setup of the Drop Test Simulation

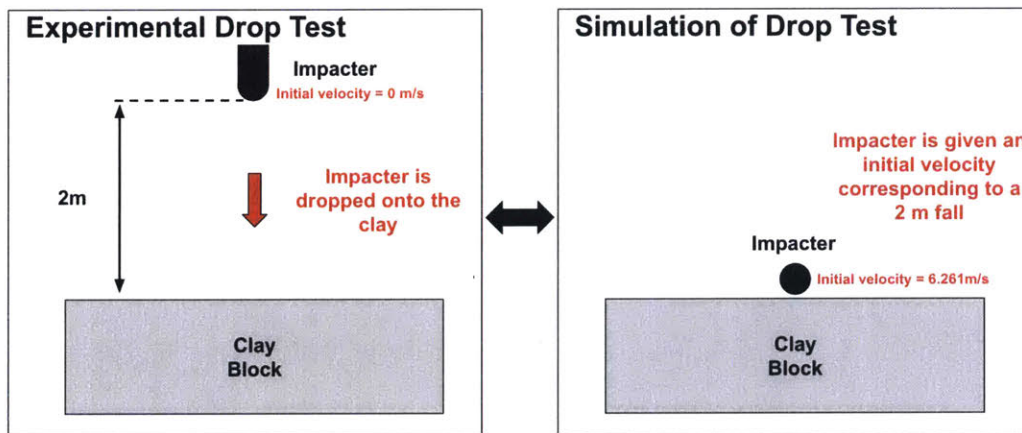


Figure 4-1: Comparison between the experimental drop test setup and the simulation setup

Figure 4-1 shows a comparison between the experimental drop test and the simulation of the drop test. To model the test, the simulation requires setup in the following three areas: the clay block including boundary conditions, the steel mass impacter and the contact between the two.

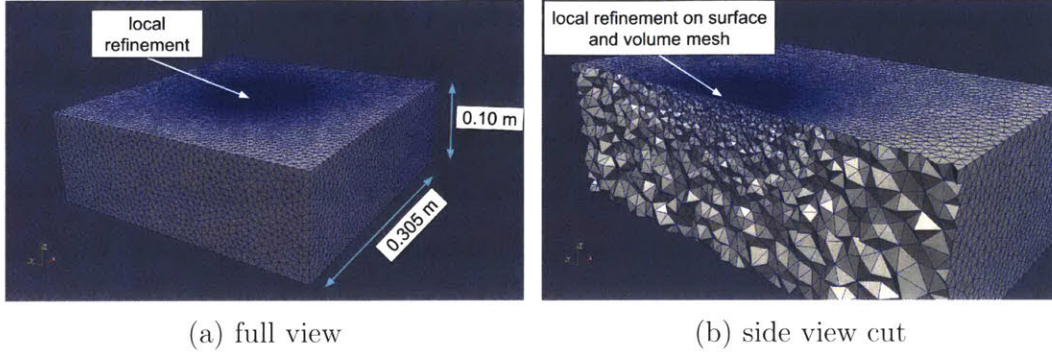


Figure 4-2: The clay block contains 262.000 tetrahedral elements with local refinement around the point of impact

A three-dimensional (3D) mesh using tetrahedral elements is created using Gmsh [34] with the exact geometry of the clay block. The boundary conditions are modeled according to the experimental boundary conditions. For experimental testing, the box containing the clay prohibits it from expanding perpendicular to the bottom and side surfaces respectively. Frictional effects between the surfaces of the box and clay during lateral movements are not observed during experimental testing in part due to the minimal amount of deformation of the clay close to the edges of the box. Thus, a roller boundary condition is chosen to model the interaction between the box and the clay. The top surface of the clay block is modeled as a free surface.

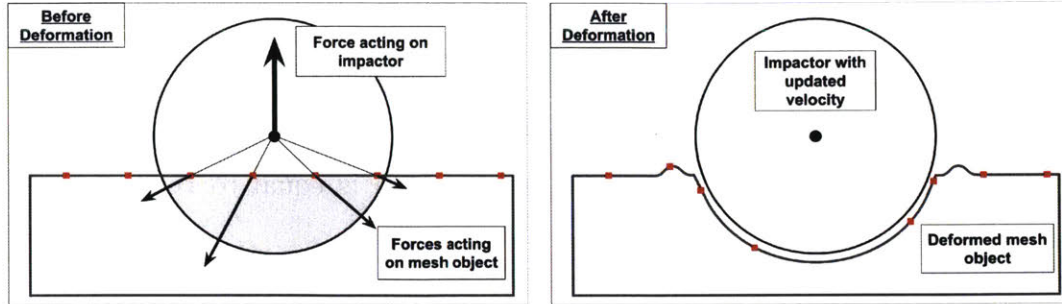
The mesh contains 262.000 linear tetrahedral elements and includes local refinement, causing it to be divided into two loosely defined regions (Figure 4-2). The first region is around the point of impact. During impact, the clay is compressed and pushed away from the impactor, forming an impact crater. The mesh experiences high-localized mesh distortion in this region. In order to accurately capture the response of the clay to the impact, this first region has been highly refined on the surface and through the volume of clay block. The second region is away from the impact crater and includes the edges of the clay block. The important role of this region is to accurately capture the effects due to the confinement roller boundary conditions. Compared to the first region around the point of impact, this second region experiences very little mesh distortion and no localized refinement is needed there.

The impacter used in experimental testing is a steel cylinder with a hemispherical end. For the drop test simulation, this impacter is modeled as a rigid sphere with a radius of 0.02225 m corresponding to the radius of the hemispherical end. The mass of the impacter used in the simulation is 1 kg, which is equal to the mass of the experimental impacter.

The initial position of the rigid sphere impacter is centered on top of the clay block, with the sphere and clay block not touching. The sphere is given an initial velocity of 6.261m/s, equal to the velocity seen by an object falling from 2m height. Gravitational effects on the impacter are included but do not affect the result of the simulation significantly, which was concluded after comparing the simulation results with gravitational effects turned off.

A difference between the experimental drop test and the simulation is the shape of the impacter (or falling mass). Using a sphere instead of a cylinder to simulate the impacter is considered acceptable because of the following reasons. First, the shape that comes into primary contact with the clay during experimental testing is the hemispherical end of the cylindrical impacter. The wall of the cylinder comes into secondary contact with the clay, mainly in the form of friction and there is some uncertainty as to how much this friction influences the final indentation depth in the clay. For the purpose of this work the frictional effects are assumed to be small and thus friction between the impacter and clay has not been implemented at the time of this work. Second, using a sphere to simulate the impacter is considered acceptable because during or after impact, the clay does not fill in over the sphere.

To simulate the contact between the impacter and clay block, the contact algorithm described in Chapter 3 is used. The contact algorithm determines the contact force between the rigid sphere impacter and the clay. At each time step of the simulation, the amount of interpenetration between impacter and clay is determined, and the contact force is applied to both bodies. As illustrated in Figure 4-3b the applied contact force results in a decrease of velocity of the impacter and a deformation of the clay.



(a) The contact algorithm determines the forces acting on the impactor and mesh (b) Applying the forces results in a decrease of the impactor velocity and a deformation of the mesh object

Figure 4-3: Illustration of how the contact between the impactor and clay is modeled using the contact algorithm

4.2 Results

The simulation results using the optimized material parameters (Table 4.1) are shown in Figures 4-4, 4-5, 4-6, and 4-7. As can be seen, the impactor pushes into the clay block, causing a significant amount of local deformation of the clay block and forming an impact crater. Due to the high amount of incompressibility of the clay, the clay bulges upwards around the point of impact and forms a mound. The final indentation depth of in the clay is 25.8 mm.

The final shape of the clay and the final indentation depth correspond to the results of a passed experimental drop test. For an experimental drop test, the clay is considered calibrated if the final indentation depth in the clay is 25.4 ± 2 mm. The final indentation depth of the simulation is 25.8 mm, which falls into that calibration window. The resulting shape of the clay after an experimental drop test shows a bulging up of the clay around the impact crater, which is qualitatively captured in the simulation results.

ρ (kg/m^3)	E	ν	P_{ref} (Pa)	V_{ref}	P_c (MPa)	η (kPa s)	Friction Angle (degrees)
1529	750	0.4	0.5	0.75	1.0	1.0	10

Table 4.1: Optimized material parameters

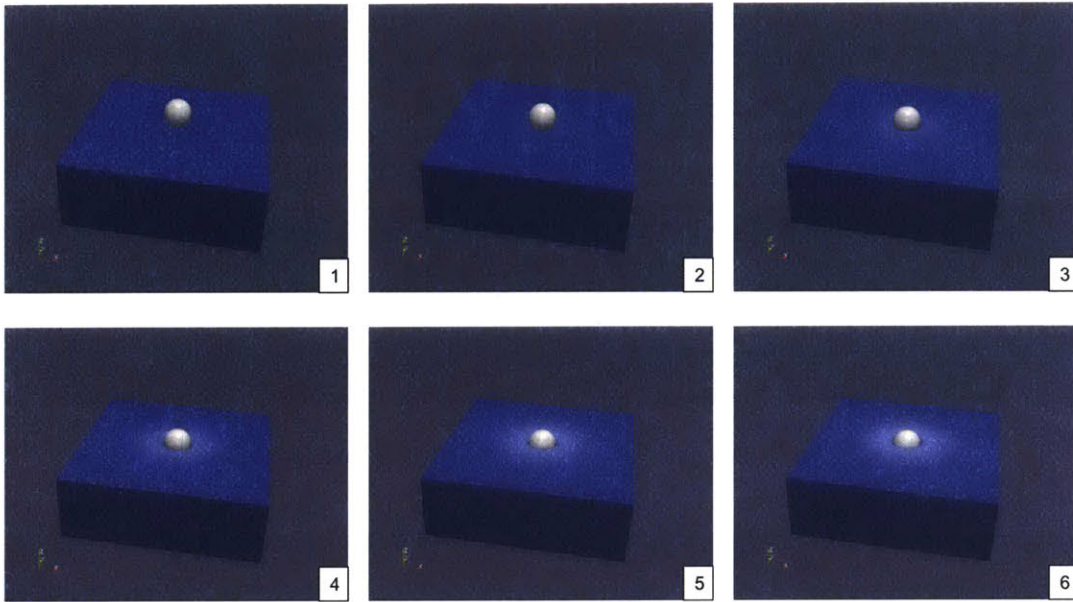


Figure 4-4: Full view of drop test simulation

Figure 4-7 shows the indentation depth in the clay vs. time in the simulation. Current efforts are underway to obtain experimental values for the drop test for the indentation depth vs. time, but they are not available at the time of this work. However, experimental values of the indentation depth in Roma Plastilina clay vs. time of similar drop test experiments exist in literature [26, 27]. Although the experimental setup and conditioning steps of the clay are different from those specified in the helmet testing protocols, these experimental results can be used as a qualitative measure of the structural behavior of Roma Plastilina clay.

The experimental indentation depth in the clay vs. time shows a gradual decrease of the rate of indentation depth with no indication of an elastic recovery of the clay. An elastic recovery of the clay would have been evident in an overshoot of the indentation depth vs. time results, which would mean that the final indentation depth after a drop test is not the maximum indentation depth in the clay. Since an elastic recovery of the clay in an experimental drop test is not observed, it is assumed that a plotted curve of the shape of the indentation depth vs. time would show a gradual leveling

off at the final maximum indentation depth.

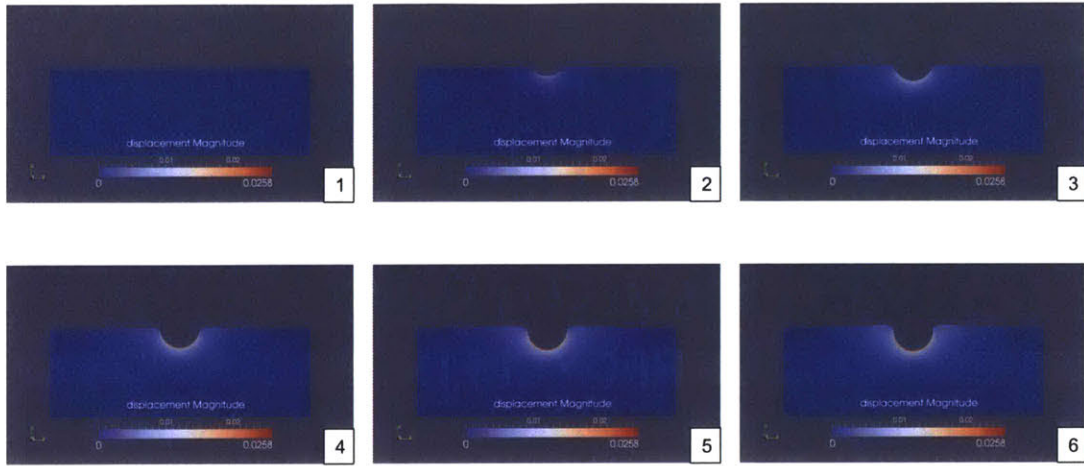


Figure 4-5: Cross section view of the drop test simulation

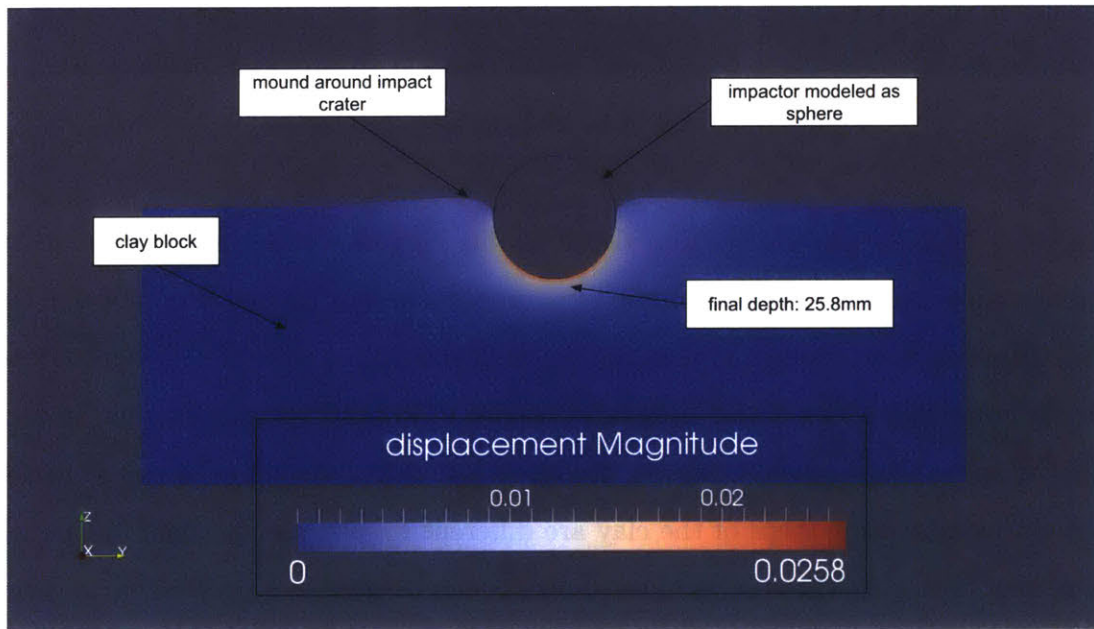


Figure 4-6: (Cross section) Final indentation depth in the clay is 25.8 mm

The quantitative measure of the final indentation depth in the clay, as well as the qualitative measures described in the previous paragraphs (mound around impact zone, indentation depth vs. time) are used to compare the simulation results with the experimental results of a drop test. They are found to be in good agreement.

As a result of the drop test simulation, the mesh experiences high-localized deformation and element distortion. As seen in Figure 4-8, deformation occurs almost

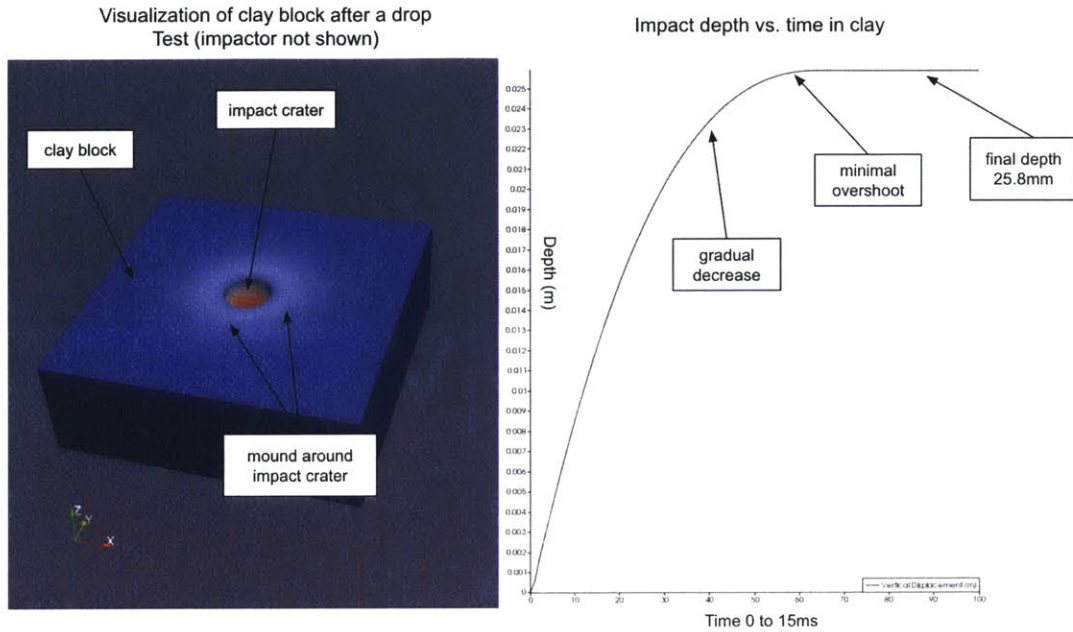


Figure 4-7: Indentation depth in the clay vs. time

exclusively at the impact region while the elements away from that region experience little to no deformation. The elements immediately at the impact region are severely distorted in order to achieve the final indentation depth of 25.8 mm. This high-localized distortion is made possible by two important features in the simulation and model setup: the use of linear elements and the loosening of the tolerance in the plastic strain convergence in the Cam-Clay constitutive model.

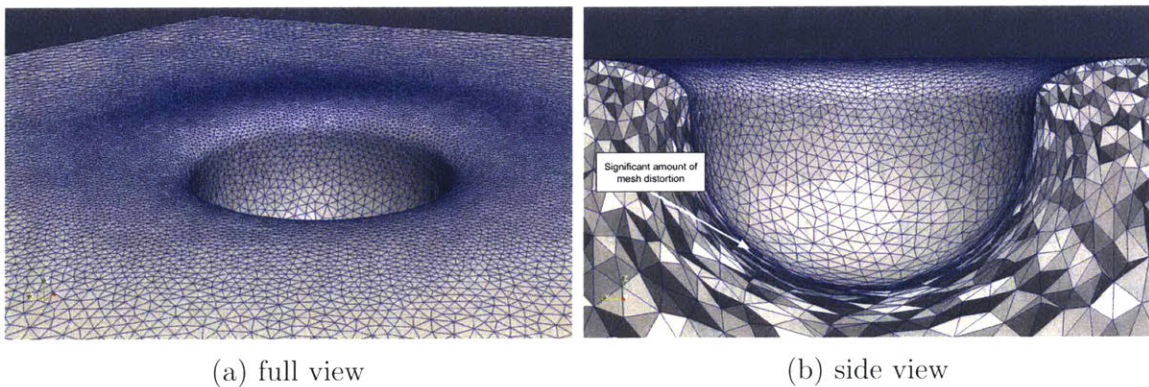
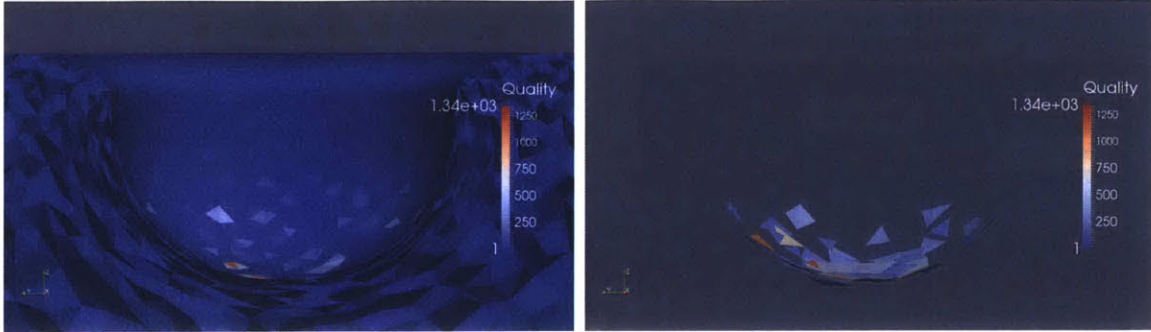


Figure 4-8: The mesh object experiences high-localized deformation and element distortion around the impact crater

The high distortion of the elements in the impact region causes a “squashing”, in



(a) Quality of elements around the impact crater (b) Poor quality elements around the center of impact

Figure 4-9: The high distortion of the elements reduces the quality of the elements severely

which the elements experience a significant reduction in volume and quality. When this reduction in volume becomes extreme, the use of linear elements prevents an interpenetration of these elements. All attempts at using higher order elements during drop test simulations failed, because the critical time step became too small or went negative. The high distortion of the elements reduces the quality of the elements severely. As seen in Figure 4-9, the quality of the elements immediately around the center of impact are orders of magnitude worse than the quality of the rest of the elements. Even while using linear elements, this reduction of quality of those elements causes the critical time step of the simulation to decrease as well, albeit at a lesser rate than while using higher order elements. Furthermore, as seen in Figure 4-9b, there are a few elements whose quality has decreased substantially more than the others. Those elements, colored in red, came close to failing, which would have caused the simulation to fail. Optimizing the mesh quality, in particular around the impact region, decreases the number of elements that end up close to failure and causes the simulation to run more smoothly.

The other feature that enables the high distortion of the elements is a loosening of the tolerance value in the plastic strain increment iteration in the constitutive model. The plastic strain increment in the model is determined using a Newton-Raphson iteration. The Newton-Raphson iteration converges on a value of the plastic strain increment, which is used to compute the plastic strain in the model. The convergence

occurs by meeting a tolerance value, which was initially set at a very tight tolerance. Initial drop test simulations continued to fail, and it was found that although the Newton-Raphson iteration had converged, it had not reached the tight tolerance value. A loosening of the tolerance value enables the model to accept the converged value for the plastic strain increment, allowing for the drop test simulation to run without failure and enabling high element distortion.

Furthermore, reducing the tolerance value is considered acceptable after comparing the results of a separate constitutive level test using different tolerance values. The hydrostatic compression test, which is used to verify the implementation of the Cam-Clay model as described in Chapter 2, is performed using a range of tolerance values. The resulting volumetric deformation curves for the tests using different tolerance values are nearly identical. Slight, oscillating deviations around the volumetric deformation curve obtained by the original tight tolerance value are observed. These oscillations around the original curve are very small and approximate the plastic strain increment well. However, for too loose tolerance values, the oscillations go unstable and the test fails. Thus, reducing the tolerance value to a certain degree is considered acceptable in providing the necessary close approximation of the plastic strain increment and enabling the drop test simulation to run.

Chapter 5

Simulations of Helmet Test Protocols

Before being delivered to the soldier, combat helmets are evaluated following the helmet test protocols [1]. These protocols specify a number of standardized experimental tests, which include ballistic and non-ballistic tests, and are performed on combat helmets in order to obtain measure of their effectiveness to stop a threat to the head. During ballistic testing, each helmet is shot five times in five separate locations (front, back, both sides, and top), and the resistance to penetration by the projectile and the helmet backface deformation signature are used as a metric to evaluate helmet performance.

In order to record and measure these two metrics, Roma Plastilina clay is used as a ballistic witness material, as described in Chapter 1. According to helmet test protocols, the helmet is placed on the Aberdeen Test Center (ATC) headform consisting of a metal frame and Roma Plastilina clay, as seen in Figure 5-1a [1]. The metal part of the headform has a base and four protruding petals, forming the overall head shape. The clay is filled into the slots between the petals and close attention is placed on matching the overall topology of the headform as described by the metal frame. The metal part of the headform with the petals is designed such that during impact in all five locations, the resulting backface deformation of the helmet primarily comes into contact with the clay, not the petals, which allows the clay to record the resulting maximum indentation depth and any potential penetration by the projectile.

There are a number of concerns with current helmet test protocols, with the

major one being that there appears to be no direct correlation between the current test metrics and head/brain injury [1]. In particular, the current threshold values for the maximum allowed indentation depth in the clay after impact seem to be mainly based on historical helmet testing precedents [1]. Other deformation results seen in the clay such as the overall shape of the impact crater and the indentation rate could also potentially be appropriate metrics to use for helmet testing.

Next to the apparent lack of injury correlation, another concern is that the maximum indentation depth in the clay may be influenced by the current headform design with the size and spacing of the metal petals potentially altering the flow of the clay during impact. Furthermore, the spacing between the petals that form the slots might be smaller than the size of the helmet backface deformation, which means that the helmet came into contact with the metal, thus reducing the maximum indentation depth in the clay. Another concern is that there is only one headform size currently used for testing all helmet sizes. This difference in helmet sizes affects the standoff distance between the helmet and headform and may further influence the resulting recorded backface deformation.

Several efforts have been proposed to redesign the headform and help address some of the before mentioned concerns [1]. One suggested alternative to the current headform design is using five different headform designs that are specialized for the impact locations. This method would eliminate the metal petals and any possible influence they may have on the backface deformation. Another suggestion to improve helmet testing methodology is to use different size headforms corresponding to the helmet sizes thus creating a consistent standoff distance between the helmet and clay irrespective of helmet size.

In an effort to further investigate these concerns and improve helmet test protocols, simulation and modeling work has been proposed. The insights gained from modeling the helmet test protocols including the headform can be used to complement experimental testing. In literature, there are a few sources that use clay as a witness material to model armor and helmet backface deformation signatures [16, 17]. Li et al. develop a simplified headform model that is based on current helmet testing protocols

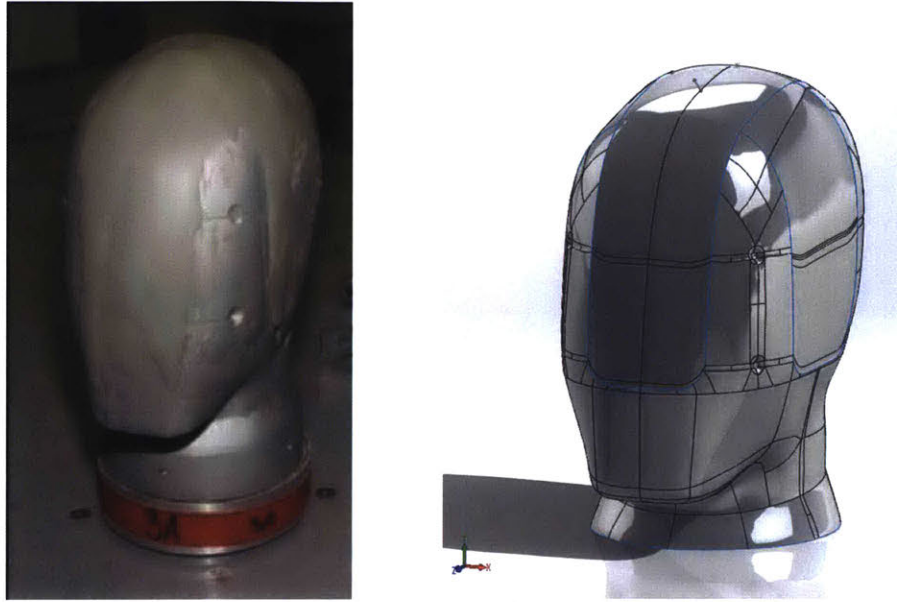
[17]. Their model includes the metal frame of the headform, Roma Plastilina clay and a helmet shell without pads. Their constitutive model for the clay is provided by a commercial code, and a separate drop test simulation is used to calibrate the given material parameters for their model. For the helmet, they use an orthotropic elasticity model along with a progressive damage model. Li et al. perform impact simulations using the headform model and are able to obtain a measure of the helmet backface deformation in the clay for three different impact locations to the helmet: frontal impact, crown impact and ride-side lateral impact.

In this work, a detailed CAD model of the headform with clay is developed using the scanned geometry data from the experimental headform. Ballistic impact simulations are performed on the full headform assembly including the metal frame, Roma Plastilina clay and a helmet with pads. The constitutive model described in Chapter 2 is used to model Roma Plastilina clay. Ballistic impact simulations using the headform assembly are performed in conjunction with simulations on a human head model. The intracranial pressure distribution in the human head is compared to the pressure distribution in the clay and the differences in the responses are highlighted. This simulation work provides a tool for future efforts at correlating deformation results in the clay to head injury and offers insights on the before-mentioned concerns regarding current headform design.

5.1 Headform and Helmet Model Creation

A full three-dimensional (3D) model of the headform test assembly is developed. The model is based on scans of the geometry of the experimental assembly and is specified in an IGES file. The IGES file contains the topological lines of the metal part of the head form and the topological surface of the clay.

Initial tries at creating a model from the IGES files using SolidWorks [35] and ANSYS [36] failed. The inability to create a model from the IGES file without any modification is due to inaccuracies in the scanned geometry. There are several



(a) Experimental headform with Roma Plastilina clay (b) Repaired SolidWorks model of the headform

Figure 5-1: Current headform shape used for helmet testing

repetitive topological lines describing the same edge of the headform, which causes them to be identified as open seams. Other topological surface features in the IGES file are either not accurately modeled as surfaces by SolidWorks and ANSYS, or are missing, creating open holes. These open seams and holes prevent SolidWorks and ANSYS to accurately recognize the headform as a solid volume. Instead, the headform is seen as a collection of individual line pieces and small faces. Furthermore, the clay part of the headform is seen as two disjointed clay surfaces. Both clay surfaces are neither connected to each other nor to the metal frame of the headform, but are floating slightly above it as seen in Figure 5-2.

Several steps are taken using SolidWorks and ANSYS in order to create a full 3D model of the headform from the IGES file. The approach is as follows:

- Focus on repairing the metal headform first (patch all the holes and seams, repair and/or replace bad faces) and create a volume
- Using the patched up metal headform as a foundation, add surfaces to create a volume for the clay and to achieve conformity between bodies

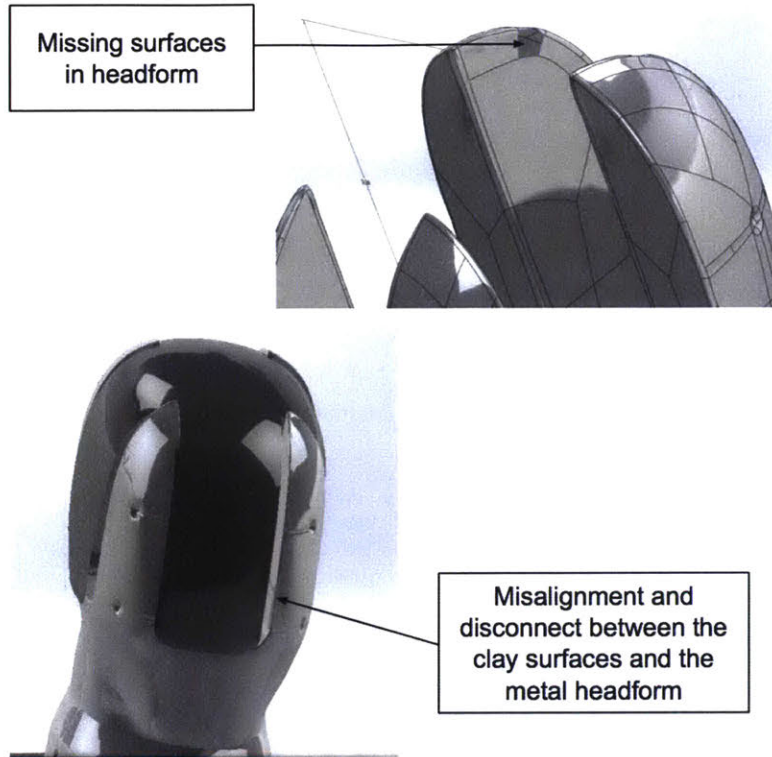


Figure 5-2: Unrepaired headform model

- Modify the added clay surfaces to match the given topology
- Add a helmet to the headform and assure mesh conformity

To repair the metal headform, SolidWorks is used to patch the larger holes and replace missing surface pieces. To do this, the SolidWorks tools "compound curve" and "boundary surface" are used. "Compound curve" lets the user combine the line pieces surrounding a hole into larger curves. The tool "boundary surface" takes these newly created compounded curves and uses them as boundary edges to create a corresponding boundary surface matching the surrounding topology. The same methodology that is used to patch the larger holes is used to repair individual intersecting faces. The tool "delete face" lets the user delete any bad faces, creating an open hole that can be patched using the above mentioned tools. These tools are also used to repair seams along the rounded edges of the headform. After all the larger bad geometry features are repaired, SolidWorks and ANSYS are used to patch the smaller features using their automated repair tools. Those tools automatically detect and repair holes

and seams, and are useful for smaller bad geometry features but often fail for larger ones.

After the above mentioned steps are performed, ANSYS is used to create a volume mesh of the metal headform. The purpose of creating this volume mesh is to verify that all the initial holes and seams have been patched and that the repair of the headform is successful. The volume mesh is shown in Figure 5-3.

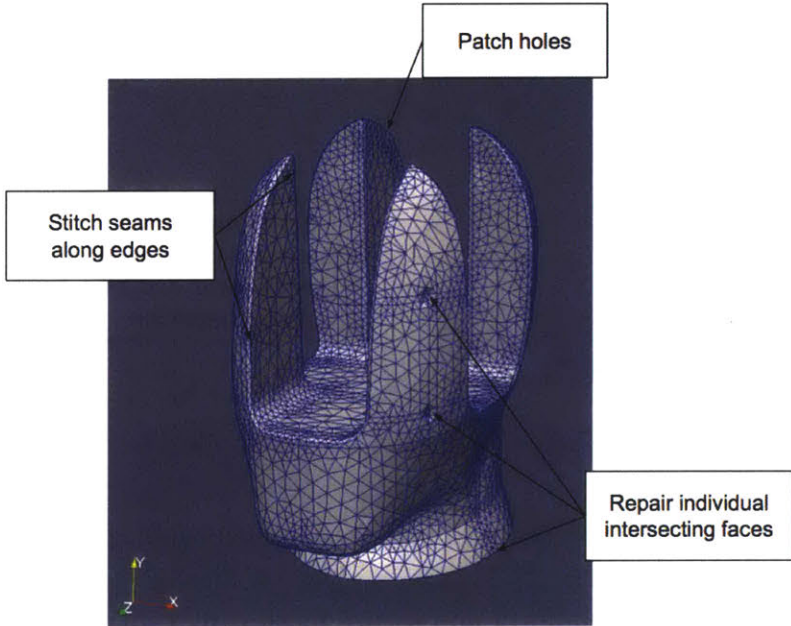


Figure 5-3: Repaired metal headform

The next step in order to create a complete model of the headform is to add the clay part. The repaired metal headform is used as a foundation to create the clay body. Similar to what happens during experimental testing, this process can be seen as filling the clay into the slots provided by the metal petals. This is achieved by using the edges of the metal headform as boundary curves and creating boundary surfaces spanning the petals. This process is very similar to the process used to patch open holes. The newly created boundary surfaces enable the creation of a bounded volume for the clay body. As seen in Figure 5-4, the clay boundary surfaces are modified accordingly in SolidWorks to match the topology of the disjointed clay surfaces provided by the IGES files. After creating the clay volume, ANSYS is used to successfully create a 3D mesh of the headform with clay, thus verifying the repair

of the model. Mesh conformity between the clay and metal is assured since they share boundaries.

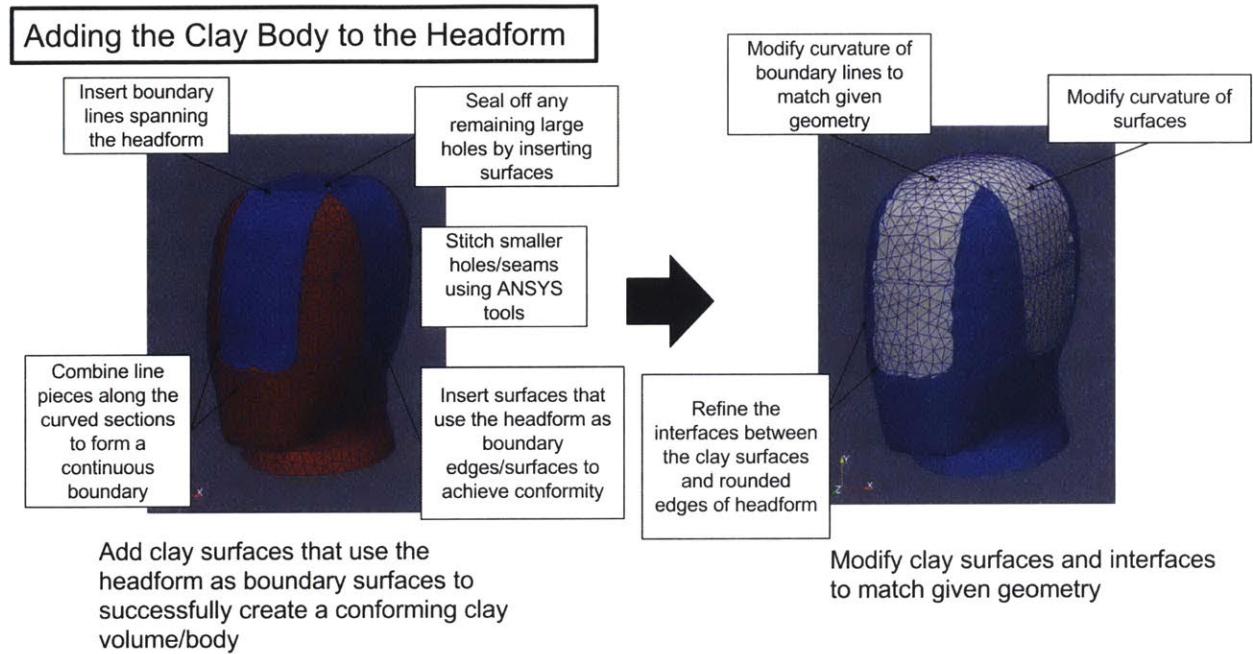


Figure 5-4: Steps detailing the process of adding clay

After the model for the headform with clay is successfully repaired, a helmet with pads is included in the model. The helmet used is a CAD model of a current combat helmet. A SolidWorks assembly involving the headform and helmet is created, and the helmet is placed on top of the headform. Close attention is put on achieving connectivity between the helmet pads and the headform. This connectivity is vital in assuring future mesh conformity between the individual mesh objects making up the helmet-pads-headform model. Connectivity is achieved in the SolidWorks assembly by placing the helmet on the headform such that the helmet pads slightly interpenetrate both the helmet and the headform. Subsequent meshing performed in ANSYS detects this interpenetration and treats the interpenetrating bodies as one continuous mesh object.

During the meshing process in ANSYS, the program assigns a separate material to each part used in the SolidWorks assembly that has a volume. This means that ANSYS recognizes the helmet shell, the individual pads, the metal part of the head-

form and the clay part of the headform as separate volumes and assigns them separate materials. ANSYS also sees the interpenetrations between the pads and the helmet shell, as well as between the pads and headform as separate materials. After meshing, the user needs to work through the list of created materials and collect them in order to form one material group for all the pads, one for the helmet, one for the metal part of the headform and one for the clay part. This involves identifying the created materials due to the interpenetrations, followed by correctly assigning which material groups they belongs to. For all the cases of interpenetration of the pads with the surrounding bodies, the created material due to this interpenetration is assigned to the other body - in the case of a helmet and pad interpenetration, the material is assigned to the helmet material; in the case of a headform and pad interpenetration, the material is assigned either to the clay or to the metal material group. The assumption here is that placing the helmet on the headform in an experimental setting would involve some compression in the pads as the weight of the helmet settles on the headform. Furthermore, it is assumed that the helmet would not be a perfect fit causing the standoff distance between the helmet shell and the headform to vary, resulting in some pads being compressed more than others. Keeping this in a mind, a “compression” of a pad in the model due to interpenetration is never greater than a few millimeters, which is a fraction of the original pad thickness (19 mm).

After correctly assigning the created materials to one of the four material groups (helmet shell, pads, metal headform, clay) the process of creating a headform assembly model with helmet is complete. The completed model for the headform assembly and mesh containing 730,000 tetrahedral elements is shown in Figure 5-5.

As can be seen in Figure 5-5, localized mesh refinement exists around small geometric features such as along edges and sharp curves. This kind of refinement is an automated process in ANSYS in order to respect detailed topological features of the model. Although a certain degree of this kind of refinement is unavoidable and desirable, the mesh for the headform contains refinement at some locations that is not needed, for example around the chin and bolt holes. The metal part of the headform experiences little or no deformation during testing and respecting the original

topology there does not affect the simulation results.

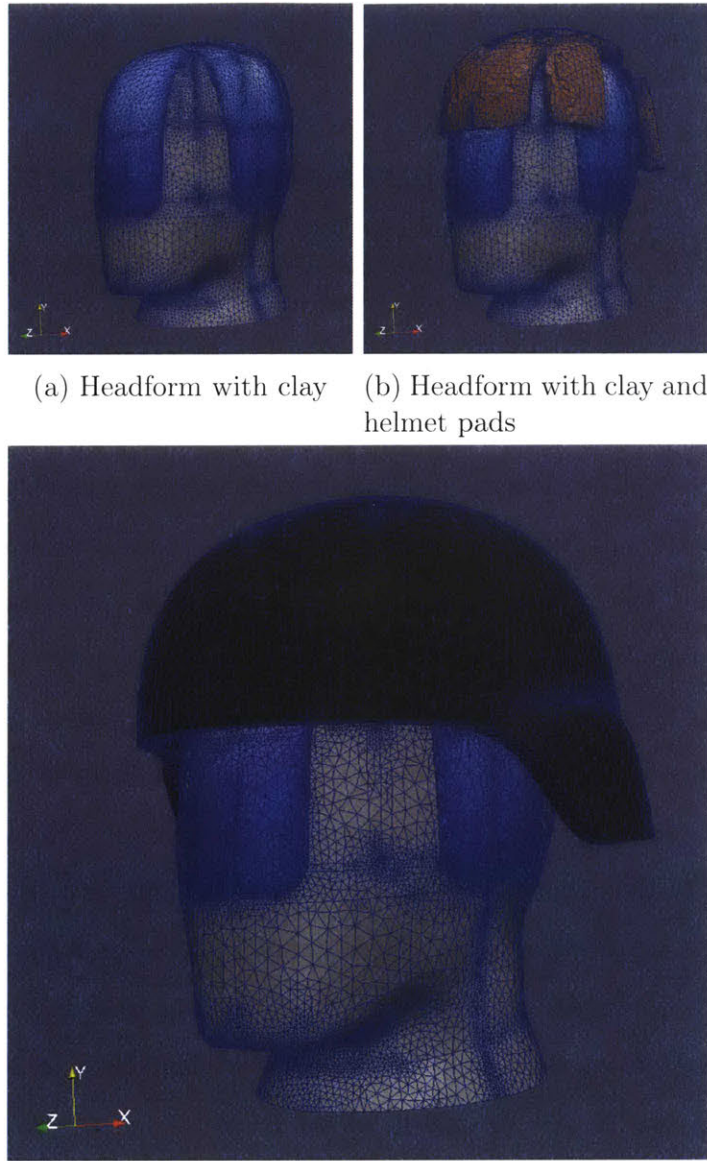


Figure 5-5: Completed model for the headform assembling including clay and combat helmet

Future improvements to the headform assembly mesh should include localized mesh refinement at the locations where an impactor strikes the helmet, and throughout the clay part of the headform. Localized refinement around the impact zone(s) and throughout the clay enables the simulation to better capture the response of the model. Furthermore, future headform assembly models should include difference helmet sizes and different helmet types. The methodology in creating the hel-

met/headform described in this work allows this flexibility and can be applied to create the different models.

5.2 Ballistic Impact Simulation to Record the Helmet Backface Deformation Signature in the Clay

In this section, a ballistic impact simulation using SUMMIT is performed on the developed headform assembly model.

As previously described, during ballistic helmet testing according to the helmet test protocols the combat helmet is shot five times in five different locations (front, back, both sides and top). The projectiles are 9 mm rounds fired from a rifle-like assembly. Ideally to simulate these ballistic impacts a model is needed that incorporates all the components necessary to capture the physics of the impact. The components would include validated constitutive models for the clay, helmet shell and helmet pads, a model for the projectile that captures all the physical characteristics of the real world bullet (shape, mass, velocity), and an algorithm to compute the contact between all objects involved, among other things. The ultimate purpose of such a simulation would be to model a real world ballistic impact to obtain validated results for the helmet deformation and backface deformation signatures in the clay.

The work presented in this document serves to lay the groundwork for achieving this purpose. To this end an important step is a proof of concept in developing the capability to model a ballistic impact to a helmet and modeling the backface deformation signature of the helmet in the clay. To reach this step, it is crucial to use a suitable constitutive model for the clay, while the model for the helmet and pads needs to only approximate their structural behavior. However, the current setup for the headform model assembly in this work provides the capability for future work to easily switch out any of the constitutive models for more complex models that are specifically designed for modeling a combat helmet and pads.

In the ballistic impact simulation described in this section the following the con-

stitutive models are used for individual components of the headform assembly. For the clay part of the headform, the Cam-Clay model described in Chapter 2 is used. The material parameters for this model are the optimized material parameters determined after calibrating the clay using the drop test, as described in Chapter 4. The optimized material parameters are shown in Table 5.1. For the metal part of the headform and for the helmet, a J2 plasticity model is used with elastic parameters similar to steel (Young's Modulus of 200 GPa, Poisson's Ratio 0.4 and density of 7830 kg/m³). The reason for choosing the J2 plasticity model for the helmet is that the model is well suited for capturing large localized (plastic) deformations expected during the impact with the projectile. For the helmet pads, a Neo-Hookean material model is used due to its ability to capture large elastic deformations with the material parameters being 8.44 MPa (Young's modulus), 0.2 (Poisson's ratio) and 61.3 kg/m³ (density). These parameters correspond to the parameter used in previous simulations with helmets performed by Prof. Radovitzky's research group to model helmet pad compression.

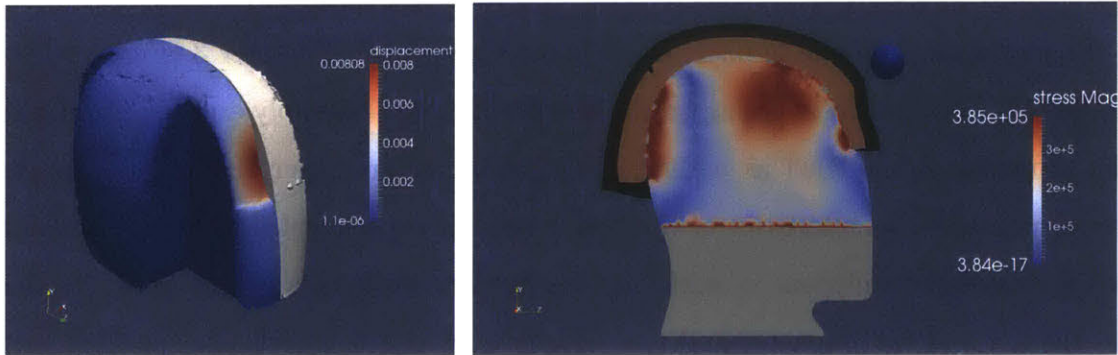
To model the ballistic impact, the contact algorithm in Chapter 3 is used to determine the contact forces acting on the headform model assembly and the projectile. The projectile is modeled as a rigid spherical impactor rather than matching the precise physical characteristics of the bullet used in experimental testing, a decision that is considered sufficient in achieving the fundamental goals of this work. To this end the mass of the impactor and the velocity at which it travels are specified such that upon striking the helmet, the impactor has enough kinetic energy to cause the helmet to deform and hit the clay underneath. The specifications of the impactor are as follows, the impactor is a rigid steel sphere with a radius of 1.5 cm travelling horizontally towards the headform assembly model at 200 m/s. A single impact to the front of the helmet is modeled and this impact location follows the helmet test protocols. The boundary conditions for the headform assembly model are fixed at the bottom and free everywhere else, and the total simulation time is 1 ms.



Figure 5-6: Frontal impact simulations are able to model the helmet backface deformation and record the deformation in the clay

ρ (kg/m ³)	E	ν	P_{ref} (Pa)	V_{ref}	P_c (MPa)	η (kPa s)	Friction Angle (degrees)
1529	750	0.4	0.5	0.75	1.0	1.0	10

Table 5.1: Material parameters used for the clay in the headform assembly model



(a) The maximum measured backface deformation signature in the clay is 8 mm. The deformed clay and the original undeformed clay are shown side by side

(b) Stress distribution throughout the clay suggests that the headform and helmet influence the flow of the clay

Figure 5-7: Simulation results in the clay

The results for the frontal impact simulations are shown in Figure 5-6. Upon impact the helmet deforms locally and deflects the impactor. The deformation of

the helmet compresses the helmet pad and leaves its backface deformation signature in the clay. Upon reaching maximum deformation, the helmet shell recovers, but leaves a plastic deformation crater in the clay. The maximum measured backface deformation signature in the clay is 8 mm, as seen in Figure 5-7a. The metal part of the headform experiences little deformation and primarily acts as a boundary for the clay. The qualitative simulation results are consistent with observations from experimental helmet testing.

As it can be seen, the simulation can successfully model a ballistic impact to the helmet, the helmet backface deformation and the recorded backface deformation in the clay. In order to validate the model using experimental helmet testing results, a better constitutive model for the helmet shell and pads are needed. Although the simulation remains un-validated to experimental helmet testing results, it offers valuable qualitative observations gained from the overall deformation behavior in the clay. The following qualitative observations can be gathered:

- The total deformation area in the clay seems to border the metal petals, suggesting they might have influenced the indentation results in the clay. This observation supports the concern in experimental helmet testing that the current headform shape affects and potentially reduces the indentation result in the clay.
- The metal part of the headform seems to be affecting the flow of the clay by affecting the stress distribution throughout the clay, as seen in Figure 5-7b. Looking at a snapshot of the cross section of the clay and showing the magnitude of the stress distribution, it is observed that stress concentrations occur at the interfaces between the clay-and-metal, and clay-and-helmet. This suggests that the part of the clay opposite the side of impact still experiences the effects from it. Furthermore, a slight push-out of the clay towards the back of the headform was observed, further supporting the concern that the shape of the metal frame influences the response of clay. The stress concentration in the clay at the interface of clay-and-helmet opposite the impact side suggests

that the helmet influences the flow of the clay as well by reducing the amount the clay that is pushed out of the headform in the back.

5.3 Comparison between Clay Deformation/Pressure and Intracranial Pressure in the Human Head

In this section, the results of two ballistic impact simulations are presented. Both simulations model a projectile impacting the top of the helmet in the location specified in the helmet test protocols. One simulation uses the headform assembly model, and the clay deformation results as well as the pressure distribution results in the clay over time are presented. The other simulation uses a model of the human head, and the intracranial pressure distribution in the brain over time is shown. Both simulations have the same setup, which allows for initial comparisons of the simulation results.

Performing two simulations side by side, one using the setup according to the helmet test protocols and the other using a human head model enables valuable results to be collected for initial and future injury correlation research. Not only does this enable the backface deformation signature recorded in the clay to be compared to pressure and deformation results in the human skull and brain, but it also allows for an inside look into what is happening in the clay and brain during impact, which is either extremely difficult or impossible to obtain experimentally.

The model of the human head with helmet was developed by the Defense and Veterans Brain Injury Center and MIT [14]. It includes a complex mesh and captures a high amount of detail of the head and brain region as seen in Figure 5-8. In past simulations, this model has been used to investigate the effect of blast pressure waves to the brain [14, 15]. It uses a Tait equation of state to model the responses of the brain tissue components and a Mie-Gruneisen/Hugoniot equation of state for the skull, which provide a suitable level of approximation of describing pressure wave propagation through the human head. The details of the material models are described in [14]. A difference between the human head model and the headform assembly model

is the type of helmets used. While the profiles of both helmets are very similar to each other, the main difference is that the combat helmet in the headform model has a slightly thicker shell than the helmet in the human head model.



Figure 5-8: The human head model captures a high amount of detail of the head and brain region

The setup for ballistic impact simulations is as follows. A steel ball with a radius of 1.5 cm and is traveling at a velocity of 50m/s downwards to impact the top of the helmet. To model the contact between the steel impacter and the helmet the contact algorithm described in Chapter 3 is used. The total simulation time is 1ms. With exception of the helmet shell, the constitutive models used for the headform assembly model are identical to the constitutive models used in the frontal impact simulation described in the previous section. For the helmet shell a NeoHookean material model is used with the material parameters of 1.24 GPa (Young's modulus), 0.36 (Poisson's ratio) and 1440 kg/m³ (density), which corresponds to the constitutive model and parameters used for the helmet shell in the human head model.

The simulation results for the clay headform are shown in Figure 5-9. The steel impacter hits the top of the helmet, causing the helmet to deform downwards and to leave its backface deformation signature in the clay. The deformation signature is shown in Figure 5-11 and the maximum magnitude of the deformation in the clay is 4.6 mm. After deforming the clay, the helmet recovers elastically. The simulation results for the human head model are shown in Figure 5-9. The steel impacter hits the top of the helmet, which causes it to deform and hit the skull. The stiff skull

bone takes the majority of the load transmitted from the helmet and pads, while only deforming slightly.

Looking at a cross section of the human head model, it is evident that although the skull bone deforms little due to the impact, the load transmitted into the brain is significant. As seen in Figure 5-10, the brain experiences intracranial pressures greater than 3 MPa, which is an indicator to suggest a possible concussion [1]. Furthermore, strong pressure gradients exist in the brain caused by pressure waves traveling through the brain and being reflected back off the skull. When looking at a cross section of the clay headform (Figure 5-10), the pressure distribution in the clay offers a different picture than the pressure distribution in the human brain model. After impact, a pressure wave travels downwards through the clay. Upon reaching the bottom of the clay body bordering the metal part of the headform, the pressure wave is reflected back upwards. The pressure waves travelling to the sides of the clay body are only partially reflected off of the four metal petals of the headform. When compared to the brain, the pressure waves seen in the clay have a more uniform and distinct shape, similar to waves seen in a pool of water after dropping a pebble into it.

Further analysis can be done on plotting the pressure values at different points in the clay and in the brain. Suitable such points need to be identified, which involves additional research on the biomechanics of the brain. The pressure curves at those points can give more insight in how the wave propagates through the brain and can show how the reflected pressure waves seen in Figure 5-10 interact with each other. The wave-interaction and resulting peak pressure values might also be a key aspect in understanding how the confinement boundary condition of the skull affects the pressure wave and can lead to efforts to redesign the clay headform to better capture this boundary condition for all impact test locations.

The brain has a complex structure and is made up of different tissues with vastly different material properties. By contrast, the clay has a uniform "structural makeup". These differences are responsible for the discrepancy of the wave speed at which the pressure waves travel. The bulk modulus of the clay is more than an order of magnitude smaller than the bulk modulus of the brain, which causes the

pressure wave in the brain to travel at a greater speed than in the clay. This should be taken into consideration when considering future more biofidelic test protocols for protective helmets.

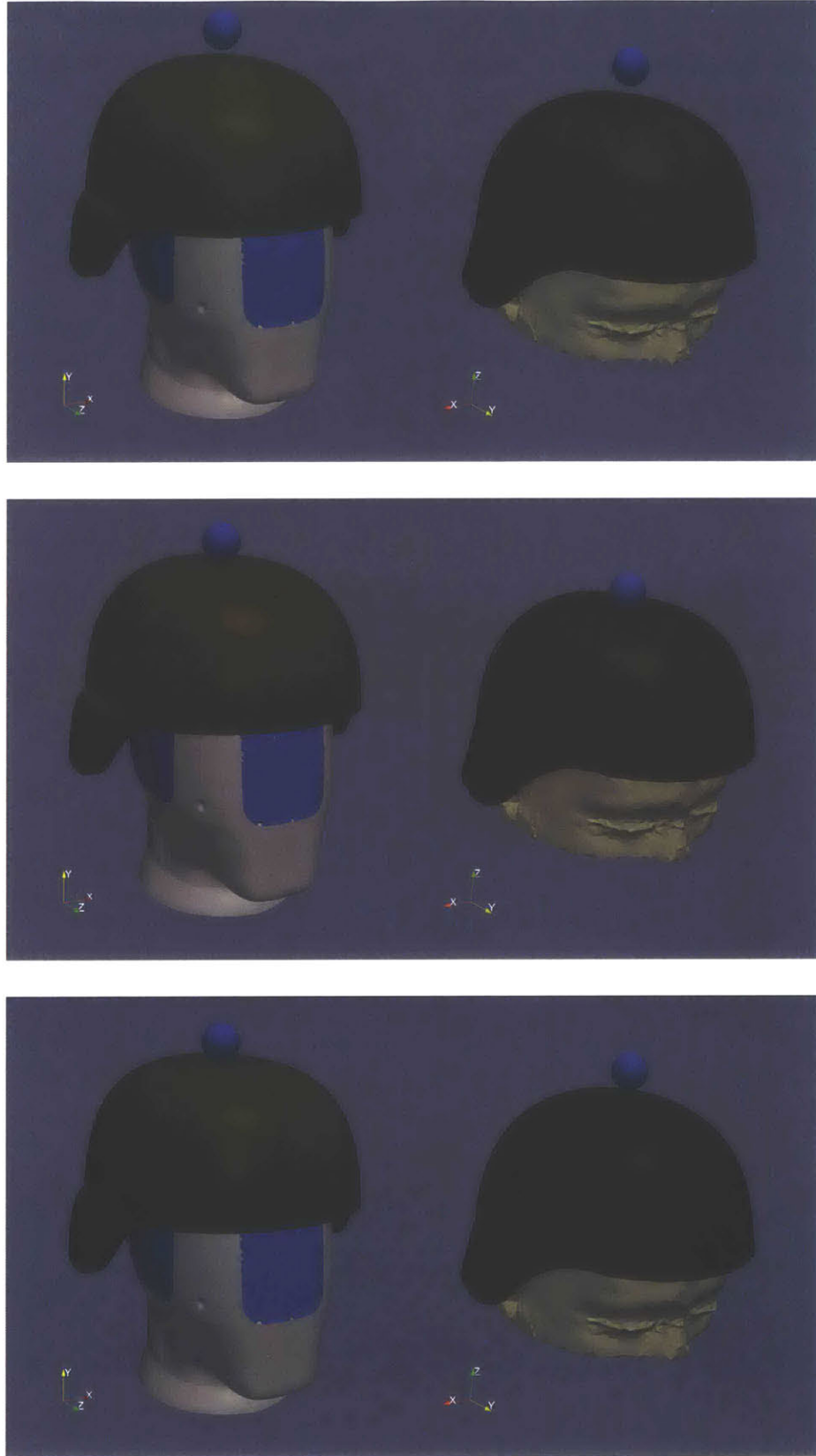


Figure 5-9: Ballistic impact simulation results for the clay headform and human head model

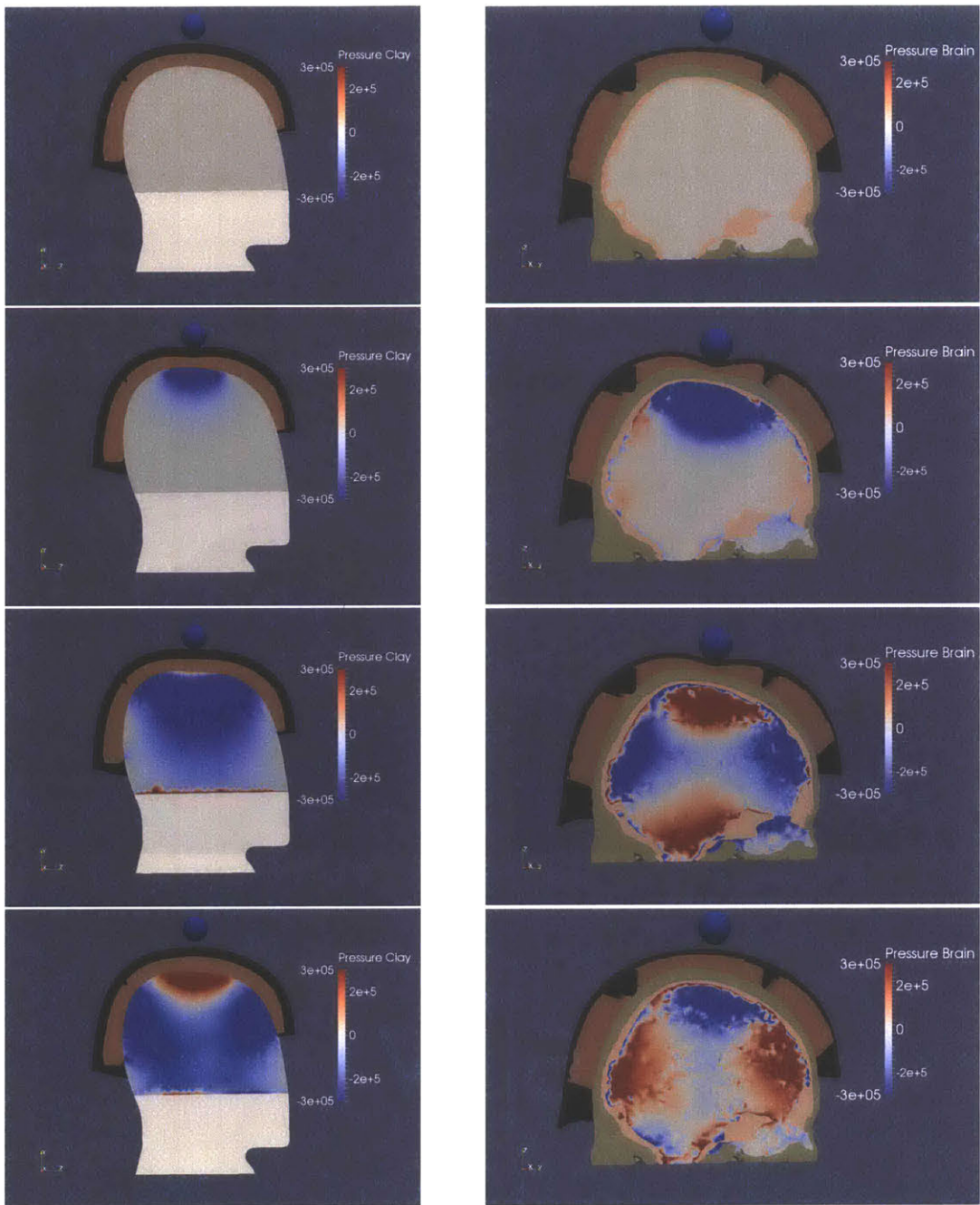


Figure 5-10: Pressure distributions as seen in cross-section images of the clay head-form and human head model

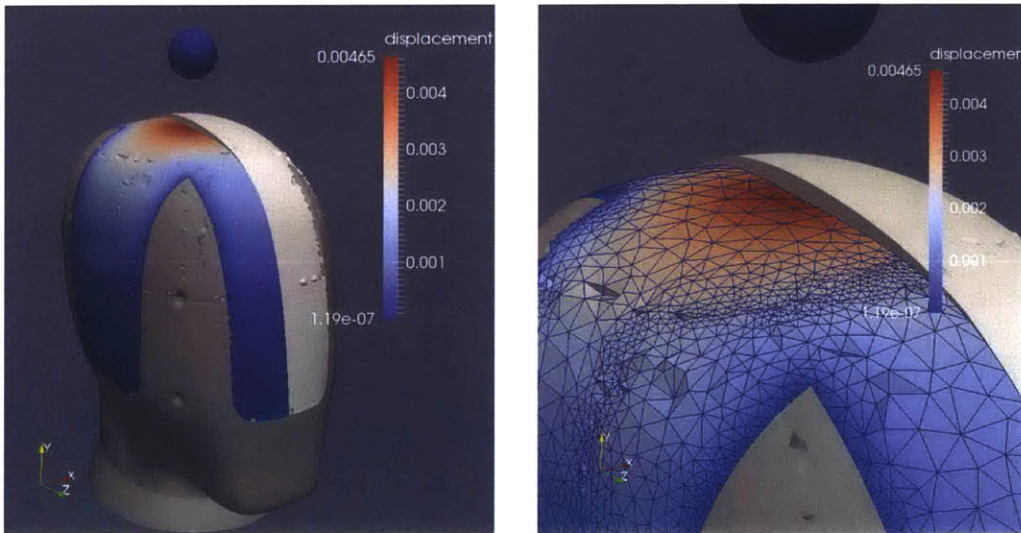


Figure 5-11: The helmet backface deformation signature captured in the clay is shown along side the original undeformed clay (helmet not shown).

Chapter 6

Conclusions

The objective of this work was to develop a comprehensive computational framework for the simulation and analysis of the helmet test protocols. To this end I have done the following:

- A material model has been implemented that is suitable to capture the structural behavior of Roma Plastilina clay. The model is based on the Cam-Clay theory and uses a variational approach to determine finite plastic deformations. Cam-Clay is used for soil like material and is able captures important characteristics seen in Roma Plastilina clay. The material model shows a high robustness and allows for high mesh distortion, which are features that are critical in order to capture the large plastic response typical for clay-like material. Constitutive level tests are performed to verify the implementation of the material model.
- A drop test simulation is used to calibrate the constitutive model for the clay. In addition to using the final indentation depth of the falling mass during an experimental drop test, qualitative indentation results vs. time and the resulting shape of the clay are used, allowing for an improved calibration of the clay model.
- Using linear elements and loosing the tolerance level by a reasonable amount significantly improves the robustness of simulations involving high mesh distortion. These adopted measures alter the simulation results only minimally.

- A detailed headform model that is based off the scanned geometry of the NIJ headform is developed. The headform model offers the flexibility to incorporate different size helmets and helmet types.
- Ballistic impact simulations on two locations (front and top) are performed on the headform model wearing a combat helmet. The simulations are successfully able to model ballistic impacts to the helmet and the helmet backface deformation signature in the clay.
- The results from these impact simulations are compared to results from impact simulations on a human head model. The intracranial pressure distribution in the human head is compared to the pressure distribution in the clay.

The following observations are gathered from the ballistic simulation results:

- The total deformation area in the clay seems to border the metal petals, suggesting they might have influenced the deformation results in the clay.
- The metal part of the headform and the helmet seem to be affecting the flow of the clay by affecting the stress distribution throughout the clay.
- The pressure distribution over time throughout both the clay headform and human head model differ significantly from each other. This is caused by a number of factors including the heterogeneous structure of the brain compared to the uniform structure of the clay, the difference in containment boundary conditions, and the difference in celerity.

The simulations and modeling performed in this work offer advanced tools to support analysis of current and future helmet test protocols. Future work can use the methodologies and tools presented in this work and build upon them for subsequent research on helmet testing.

While the constitutive model used in this work displays the strong capability to model the structural response of Roma Plastilina clay, additional tests and data should be used to further calibrate the material model. Regarding using the drop test

as a calibration test, accurate experimental indentation depth vs. time data in the clay should be incorporated. Furthermore, the use of surface geometry scans to measure the crater in the clay around the point of impact would offer more quantitative data on the shape of the clay. Next to the drop test, additional tests with higher strain rates should be used to calibrate the constitutive model. These tests could include a ballistic impact test on a flat metal plate backed by clay. The experimental indentation depth in the clay vs. time and the shape of the clay due to the backface deformation of the metal plate could be used to calibrate the clay to strain rates occurring during ballistic testing.

Besides further calibrating the clay, future work should include using more appropriate constitutive models for the helmet and pads that can more accurately capture their responses and that enable a future validation of the simulation results to take place.

The tools and models presented in this work could also contribute to research on developing transfer functions and scaling laws. The deformation results obtain in the clay during helmet testing could be correlated to injury to the human head via such transfer functions.

Bibliography

- [1] Committee on Review of Test Protocols Used by the DoD to Test Combat Helmets, Board on Army Science and Technology, Division on Engineering and Physical Sciences, and National Research Council. *Review of Department of Defense Test Protocols for Combat Helmets*. National Academies Press, 2014.
- [2] D. F. Moore, R. Radovitzky, L. Shupenko, A. Klinoff, M. S. Jaffee, and J. M. Rosen. Blast physics and central nervous system injury. *Future Neurology*, 3:243–250, 2008.
- [3] Committee To Review The Testing of Body Armor Materials for Use by the U.S. Army, National Research Council, Board on Army Science and Technology, and Division on Engineering and Physical Sciences. *Phase I Report on Review of the Testing of Body Armor Materials for Use by the U.S. Army: Letter Report*. National Academies Press, 2009.
- [4] National Research Council, Division on Engineering and Physical Sciences, Board on Army Science and Technology, and Committee to Review the Testing of Body Armor Materials for Use by the U.S. Army – Phase II. *Testing of Body Armor Materials for Use by the U.S. Army-Phase II: Letter Report*. National Academies Press, 2010.
- [5] National Research Council, Division on Engineering and Physical Sciences, Division of Behavioral and Social Sciences and Education, Board on Army Science and Technology, Committee on National Statistics, and Committee on Testing of Body Armor Materials for Use by the U.S. Army - Phase III. *Testing of Body Armor Materials: Phase III*. National Academies Press, 2012.
- [6] National Institute of Justice. NIJ Standard 0106.01 For Ballistic Helmets. *U.S. Department of Justice*, 1981.
- [7] R. Prather, C. Swann, and C. Hawkins. Backface Signatures of Soft Body Armors and the Associated Trauma Effects. Technical report, Aberdeen Proving Ground, 1977.
- [8] E. Hanlon and P. Gillich. Origin of the 44-mm behind-armor blunt trauma standard. *Military Medicine*, 177:333–339, 2012.
- [9] U.S. Department of Justice. NIJ Standard 0101.06 Ballistic Resistance of Body Armor. *National Institute of Justice*, 2008.

- [10] M. Wilhelm and B. Cynthia. Injuries to law enforcement officers: The backface signature injury. *Forensic Science International*, 174:6–11, 2007.
- [11] C. Hernandez, A. Maranon, and I. Ashcroft. Inverse methods for the mechanical characterization of materials at high strain rates. *EPJ Web of Conferences – DYMAT 2012 10th International Conference on the Mechanical and Physical Behaviour of Materials under Dynamic Loading*, 26, 2012.
- [12] U.S. Army P.E.O. Solider, ATC. Clay Handling Procedures. Technical report.
- [13] D. Bentz, A. Forster, K. Rice, and M. Riley. Thermal Properties and Thermal Modeling of Ballistic Clay Box. Technical report, National Institute of Standards and Technology – U.S. Department of Commerce, 2011.
- [14] D. F. Moore, A. Jerusalem, M. Nyein, L. Noels, M. S. Jaffee, and R. Radovitzky. Computational biology, modeling of primary blast effect on the central nervous system. *NeuroImage*, 47:T10–T20, 2009.
- [15] M.K. Nyein, A.M. Jason, L. Yu, C.M. Pita, J.D. Joannopoulos, D.F. Moore, and R.A. Radovitzky. In silico investigation of intracranial blast mitigation with relevance to military traumatic brain injury. *Proceedings of the National Academy of Sciences*, 107:20703, 2010.
- [16] J. Roberts. Assessing Behind Armor Blunt Trauma in Accordance With the National Institute of Justice Standard for Personal Body Armor Protection Using Finite Element Modeling. *Journal of Trauma*, 62(5):1127–1133, 2007.
- [17] Y. Q. Li, X. G. Li, and X.-L. Gao. Modeling of Advanced Combat Helmet Under Ballistic Impact. *Journal of Applied Mechanics*, 82:111004–(1–9), 2015.
- [18] M. Ortiz and A. Pandolfi. A variational Cam-clay theory of plasticity. *Computer Methods in Applied Mechanics and Engineering*, 193:2645–2666, 2004.
- [19] A. Schofield and P. Wroth. *Critical State Soil Mechanics*. McGraw-Hill, London, 1968.
- [20] K. Roscoe and J. Burland. On the generalised stress-strain behaviour of "wet" clay. *Engineering Plasticity*, Cambridge University Press, 1968.
- [21] Brandon Talamini and Raúl Radovitzky. A discontinuous galerkin method for nonlinear shear-flexible shells. *Computer Methods in Applied Mechanics and Engineering*, 303:128–162, 2016.
- [22] A. Seagraves and R. Radovitzky. *Dynamic Failure of Materials and Structures*, chapter 12 Advances in Cohesive Zone Modeling of Dynamic Fracture, pages 349–405. Springer, 2009.

- [23] R. Radovitzky, A. Seagraves, M. Tupek, and L. Noels. A scalable 3D fracture and fragmentation algorithm based on a hybrid, discontinuous Galerkin, Cohesive Element Method. *Computer Methods in Applied Mechanics and Engineering*, 200:326–344, 2011.
- [24] L. Noels and R. Radovitzky. A general discontinuous Galerkin method for finite hyperelasticity. Formulation and numerical applications. *International Journal for Numerical Methods in Engineering*, 68(1):64–97, 2006.
- [25] L. Noels and R. Radovitzky. An explicit discontinuous Galerkin method for non-linear solid dynamics. Formulation, parallel implementation and scalability properties. *International Journal for Numerical Methods in Engineering*, 74(9):1393–1420, 2007.
- [26] M.F. Buchely, A. Maranoncor, and V.V. Silberschmidt. Material model for modeling clay at high strain rates. *International Journal of Impact Engineering*, Accepted, 2015.
- [27] C. Hernandez, M.F. Buchely, and A. Maranon. Dynamic characterization of Roma Plastilina No.1 from Drop Test and inverse analysis. *International Journal of Mechanical Sciences*, 100:158–168, 2015.
- [28] H. Sofuoglu and J. Rasty. Flow behavior of Plasticine used in physical modeling of metal forming processes. *Tribology International*, 33(8):523–529, 2000.
- [29] T. Altan, H. Henning, and A. Sabroff. The Use of Model Materials in Predicting Forming Loads in Metalworking. *Journal of Engineering for Industry*, 92(2):444–451, 1970.
- [30] J. Atkinson. *Foundations and Slopes: An Introduction to Applications of Critical State Solid Mechanics*. McGraw-Hill, London, 1981.
- [31] M. Ortiz and L. Stainier. The variational formulation of viscoplastic constitutive updates. *Computer Methods in Applied Mechanics and Engineering*, 171(3–4):419–444, 1999.
- [32] R. Radovitzky and M. Ortiz. Error estimation and adaptive meshing in strongly nonlinear dynamic problems. *Computer Methods in Applied Mechanics and Engineering*, 172(1–4):203–240, 1999.
- [33] P. Wriggers. *Computational Contact Mechanics*. Springer, Berlin, 2006.
- [34] C. Geuzaine and J.-F. Remacle. Gmsh: a three-dimensional finite element mesh generator with built-in pre- and post-processing facilities. *International Journal for Numerical Methods in Engineering*, 79(11):1309–1331, 2009.
- [35] SolidWorks v. 2012, Dassault Systems SOLIDWORKS Corp.
- [36] ANSYS Academic Research, Release 15.0, ANSYS, Inc.